AD 422055

SD-TDR-62-

(5) 243-610

(6)

INVESTIGATIONS OF OPTICAL CROSS-SECTIONS FOR LASER-RADAR,

TECHNICAL DOCUMENTARY REPORT NO. ASD-TDR-62-726

(March 1962)

(9) Rept. for 13 mar 61 - 1 mar 62,

Navigation and Guidance Laboratory
Aeronautical Systems Division
Wright-Patterson Air Force Base, Ohio

Project No. 1670-5099, Task No. 5099-50329

(10) by (Prepared under Contract No. AF 33(616)-8169
by the University of Dayton Research Institute.
Werner R. Rambauske and Donald L. Roettele)

FOREWORD

This report was prepared by the University of Dayton under United States Air Force Contract AF 33(616)-8169. The contract was initiated by the Navigation and Guidance Laboratory of the Avionics Division, Wright Patterson Air Force Base, Ohio, with Mr. J. Pasek (ASRNGE-2) as project engineer.

This report covers a period of work from 13 March 1961 to 1 March 1962 under the subject heading "Analysis of IR/OPT Seeker Performance, Available Components and Missile Requirements."

Original data for this investigation are indexed in data books AF 33(616)-8169 located in the files of the University of Dayton Research Institute.

In addition to Mr. J. Pasek, the University of Dayton Research Institute is pleased to acknowledge gratefully the assistance of Mr. Sirons from ASRNGE-2.

ABSTRACT

Areas for detailed investigation in the field of optical radar with a Laser light source were delineated. The problem of optical reflectivity and depolarization by targets of different shape and materials is considered to be of great importance since the optical cross-section of the target is a primary part of any derived optical radar equation. Analytical and experimental results for the determination of optical cross-section are reported. The numerical determination for an optical radar equation by measurement of other important parameters has been started.

TABLE OF CONTENTS

LIST OF FIGURES

LIST OF FIGURES (Cont'd)

1. INTRODUCTION

The original intention of the work described below was to derive a general equation for the optical radar. This would be analogous to the known Radar equation valid for microwaves, and would allow the calculation of the ultimate range and radial velocity when the parameters of the system are known numerically. After study of the problems involved, various areas could be defined which were at that time (August 1961) in need of further investigation. They are summarized in the following paragraph of this report. The great complexity of these problems necessitated a limitation of the program to an investigation which was not only acknowledged to be of main importance, but likewise to be of such a nature that it could be conducted with a limited number of personnel and facilities. For these reasons, the investigations were concentrated on the determination of the optical reflection and depolarization from various targets under illumination with monochromatic, coherent, and polarized light. However, even this program was limited to an experimental determination of these parameters first with ordinary light illumination for the sake of comparison and correlation. Later on Laser illumination should be investigated. These experiments are still in progress. Moreover, measurements of many performance parameters of the Laser transmitter and receiver were started and should be continued.

2. PROBLEM AREAS FOR AN OPTICAL RADAR EQUATION

Initial considerations were divided into the following problem areas:

A) Laser-Transmitter
B) Target optical cross-section
C) Receiver performance
D) Background influence
E) Beam qualities in transmitting medium
F) Motion between transmitter, target, receiver

From one point of view, a great amount of experimental data and theoretical knowledge about the optical parameters of the optical radar system exists which permits fair estimates of its potential performance. On the other hand, as soon as one tries to define these parameters numerically with accuracy and confidence, which is necessary for the determination of ultimate performance, it becomes clear

that we are lacking the knowledge in most of the important data, relationships, and complete understanding of the involved principles.

Specifically, in a first approach to determine ultimate capabilities of the system, the following problems in the six areas of investigation (A) to (F), mentioned above, arise.

A) 1) What is the photometric intensity distribution over the cross-section of the laser-orifice as function of position and time?

2) Are the spectral width and the line contour changing in time with parameters such as coatings, heat, carburization, etc.?

3) Are the degrees of polarization and coherence constant, and what are their exact values?

4) How many and which modes of vibration actually contribute to the integrated laser-output?

5) What are the fluctuations (longer periodic oscillations) and the short periodic peak and average noise values of these characteristic parameters (intensity, spectral density, and coherence) for the wavefront emerging from the Laser?

B) 1) What are the actual sizes and shapes of targets which can be expected?

2) Are the coefficients of reflection and absorption of different materials which are employed for outer surfaces of targets the same for highly coherent and linearly polarized light as for ordinary light?

3) When can we expect deviations from Lambert's Law, and what will be the ratio of diffusely to orderly reflected light?

4) What will be the influence of interference layers, with which the target might be coated for the purpose of temperature control? What are the means of distinguishing a target, and how effective are they?

5) Is excitation of luminescence in shorter distances possible? Will scattering change the spectral characteristic and wavelength of the reflected light?

6) Will the degree of polarization and coherence be altered by the reflection process?

C) The nominal data for photocathodes seem to be insufficient for determination of ultimate performance, since the usually quoted quantum efficiency depends upon the fairly well known actual number of light quanta stochastically absorbed in a certain depth of the thin cathode layer which transforms these quanta into emittable electrons. This depth, likewise, is only fairly well known. Reemission, reflection, interference, and scattering processes take place both for the light quanta and the electrons.

1) What, then, is the capability of a photoelectric detector to distinguish signal from noise when illuminated with light of extremely high coherence and monochromaticity?

2) How much of the information contained over the cross-sectional area and time in the entrance plane of the detector is lost in different detector systems on its way to its final recording, presupposing that the optical information in this entrance plane is theoretically known. (This information cannot be known experimentally since this would already presuppose a real detector which is understood in every detail.)

D) 1) What is the background radiation and its noise influence when received by different detector systems? A distinction has to be made between star and solar emission, and earth, moon and planet reflection, and atmospheric scattering.

2) What is the probability of receiving light in one or several very small spectral bands? Can coherence and polarization be a sufficient discriminator between background and target acquisition without losing ultimate sensitivity, or will beam modulation be more effective for this purpose?

E) 1) It might be questionable whether the cross-sectional and timewise intensity distribution in a beam of small diameter and excessive length can be considered as a simple diffraction pattern and can be calculated with Fresnel theory for diffraction by a circular aperture. Since the boundary conditions

for such a beam cannot easily be formulated, an experimental approach seems to be advisable.

2) Ultimate sensitivity conditions ask for the existence of single quanta. Space is not a perfect vacuum, hence the interaction of the radiation with space particles will alter intensities calculated by classical methods. Moreover, magnetic fields may introduce slight changes in polarization angle.

F) 1) Motion between transmitter-receiver on one side and the target on the other side is of tangential and radial nature. Fast changes in tangential motion will occur when the transmitter-receiver system oscillates only very slightly around the line of sight to the target. And, if the target oscillates around this line, the parameters determining its reflective cross-section may change substantially.

2) In acquisition and detection problems usually some kind of scanning is involved. This results in questions concerning the dwell time of the beam on the target, the maximum scanning frequency possible, and possible cross-sectional deformation of the beam by aberration.

3) The radial component of relative motion produces a Doppler shift of the narrow spectral band or bands reflected from the target. What is the amount and the influence of such a shift on all the parameters mentioned above, and the ultimate sensitivity of the different detector systems?

These various questions and many others not yet defined enter the task of the program in addition to the multitude of solutions already available by publications. Since, obviously, all of these problems could not be investigated at the same time, point (B), the optical cross-section of the target, was selected as the most important.

3. GENERAL CROSS-SECTION CONSIDERATIONS

In optical reflectivity measurements, distinctions have to be made as to whether the radiation incident on the reflector is parallel or is coming from all

directions, whether it is polarized or not, monochromatic or polychromatic, and, as we believe, whether it is coherent or not. The reflector, on the other hand, will be one of either strong or weak absorption; it will reflect orderly or diffusely, and in the latter case according to Lambert's Law or not; it may be a selective reflector for certain spectral bands; it might be excited to self-emission and it may change the state of polarization of the incident radiation. In all cases the coefficient of reflectivity should measure, under defined geometrical conditions, the ratio of reflected to incident intensity when measured in photometric units, or of reflected to incident power when measured in radiometric units.

In optical radar measurements the illumination incident on this reflecting target will be in form of a parallel monochromatic beam. The surface material of the reflector, however, can exhibit any of the properties of reflectivity distinguished above, and different materials and different angles of incidence for the surface of one single target can result in various optical cross-sections. Therefore, an important part of the theoretical investigations is the task of formulating a relation for the cross-section which contains general and individual probability terms. These should be tabulated and cross-section values provided for the most probable forms, surface materials and surface material combinations.

It should be recalled that Fresnel's equations are only applicable in a simple way for the case of weak absorption (high transmissivity, i.e., glass) and smooth surfaces where the most important factor for the determination of reflectivity is the refractive index (n). In case of strong absorption (no transmissivity, i.e., metal), where the light wave only penetrates a layer thinner than a wavelength, the reflectivity for smooth surfaces is mainly determined by the refractive index (n) and the coefficient of absorptivity (xn). However, because of the strong damping of the wave in the absorbing layer, the index n and the absorptivity become a function of the angle of incidence; and the angle of polarization valid for weak absorption is replaced by a main angle of incidence (reflection of the electric vector parallel to the plane of incidence is a minimum). The complication can be seen from the fact that for metallic reflection

$$k = \frac{\sin\phi \sin 2\psi}{\sqrt{1 - \sin^2\phi \sin^2 2\psi}}$$

$$n = \tan \phi \sqrt{1 - \sin^2 \phi \sin^2 2\psi}$$

where ϕ is the main angle of incidence and ψ is the arctangent of the ratio of the reflected electric vectors parallel and normal to the plane of incidence at this angle.

Now ϕ and ψ change slightly from area to area of the same metal, and over a period of time by chemical and other molecular changes within the thin layer where the absorption takes place. This complication is the reason why even the most careful measurements are only reproducible within ten or more percent. In the case of diffuse reflection, conditions are even worse since at least three distinct phenomena should be considered: first, the orderly reflection of strong absorbing materials given by particles of the diffusely reflecting surface of a size of from one to ten wavelengths; second, the Rayleigh and Mie-scattering of particles smaller and somewhat larger than the wavelength; third, the diffraction caused by the edges and boundaries of these particles. The variability of these effects is very large. Hence, the empirical approach is the only approach which will lead to usable solutions and must be preferred over theoretical calculations.

The work in the cross-section measurement program is, therefore, divided into the following investigations:

1) The improvement of accuracy and reproducibility from one experiment to the next.
2) The use of plane polarized light and the comparing of the cross-sections with that for unpolarized light.
3) The use of optical filters and measuring of the cross-sections for several wavelength bands. This will necessitate the use of a much stronger light source.
4) The setting up of an experiment where the optical cross-sections of some simple bodies are measured using the Laser as a light source.
5) The theoretical optical cross-section for perfectly diffusely reflecting bodies can be scaled to larger bodies by some characteristic area of the body such as the projected area of a sphere or cylinder or by the base area of a cone. For a perfectly specular type body there will be a non-zero cross-section only if a portion of its surface is nearly normal to the incoming light. If ρ_1 and ρ_2 are the

principle radii of curvature of the body at this point, then the optical cross-section is given as

$$\sigma = a\pi\rho_1\rho_2$$

if ρ_1 and ρ_2 are both small in comparison to the range. For a cylindrical body ($\rho \approx \infty$) then, it is $\sigma = 2a\pi\rho$, if ρ is small in comparison to R, and for a flat plate ($\rho_1 = \rho_2 = \infty$), it is $\sigma = 4\pi R^2$. There appears to be a problem in scaling the data for an arbitrary specular body since the type of scaling will depend to a great extent on the type and number of specular points on the body. On the other hand, every target will have a certain amount of diffuse characteristics and therefore will have a cross-section at angles of incidence other than the specular point. However, the high cross-sections due to specular places on a body would probably not be counted on in actual usage (optical radar) since they are sharp and narrow spikes; rather, the continuous (diffuse) type of cross-section which can be scaled by some effective area would be used and the spikes merely added to the overall effect.

4. OPTICAL CROSS-SECTION (CALCULATED)

The optical cross-section (σ) for a body can be defined as that effective area which, if it absorbed all the power (p_i) per unit area incident upon it and radiates this energy (σp_i) isotropically ($4\pi R^2$), would result in the measured or computed power (p_R) per unit area at the receiver. In equation form

$$p_R = \frac{\sigma p_i}{4\pi R^2}$$

$$\sigma = 4\pi R^2 \frac{p_R}{p_i} = 4\pi R^2 \quad \frac{\text{Reflected power/unit area at receiver}}{\text{Incident power/unit area at target}}$$

This is entirely equivalent to the definition given in texts concerning radar-systems where:

$$\sigma = 4\pi \frac{\text{Reflected power/unit solid angle}}{\text{Incidence power/unit area}}$$

The cross-section of a simple body will, in general, depend quite strongly on its orientation with respect to the receiver and its coefficient of reflectance (a).

The cross-sections of a few simple bodies were computed. The targets are assumed to be at such large ranges that the incidence radiation can be considered plane and it is presupposed that either simple equal angle reflection or Lambert Law reflection occurs for specular or diffuse surfaces, respectively.

4.1 Cross-Section of Diffuse Simple Geometric Bodies

The equation for the diffuse energy reflected from a body takes on a simple form when the energy is computed for a very distant receiver in the same direction as the incoming radiation. This certainly will be the case for most radar type applications. If p_i is the incident power per unit area, then ($a\, p_i\, ds \cos\beta$) is the total energy diffusely reflected from the elemental surface ds which is at an angle β to p_i. The surface reflectivity (diffuse reflection coefficient) is indicated by "a". Of this power, a fraction $(\cos\beta)/\pi$ goes back in the direction β per unit solid angle. Now a unit area at the receiver subtends an angle of $1/R^2$ steradians. Hence, the power per unit area incident at the receiver is

$$p_R = \int_S a\, p_i\, ds \cos\beta \frac{\cos\beta}{\pi} \frac{1}{R^2} \qquad \pi R^2 >> S$$

$$= \frac{p_i}{R^2} \int_S a \cos^2\beta\, ds\,.$$

Since the optical cross-section is defined as $\sigma = 4\pi R^2 \frac{p_R}{p_i}$ we obtain

$$\sigma = 4 \int_S a \cos^2\beta\, ds \qquad \pi R^2 >> S$$

where the integration is taken over the entire surface as seen from the receiver at very large distances.

Only bodies which can be considered as pure Lambert diffusers of constant reflectivity, a, were considered. The following summarizes the theoretical optical

cross-sections for a number of simple geometrical shapes.

1. Sphere $\sigma = \frac{8}{3} a\pi r^2$

2. Flat Plate (no edges) $\sigma = 4a A \cos^2 \beta$ $\quad 0 \leq \beta \leq \frac{\pi}{2}$

3. Cylinder (no ends) $\sigma = 2a \pi r \ell \cos^2 \beta$ $\quad 0 \leq \beta \leq \frac{\pi}{2}$

4. Hemisphere (no bottom) $\sigma = \frac{8}{3} a\pi r^2 \left(1 + \frac{\sin 2\beta - 2\beta}{2\pi}\right)$ $\quad 0 \leq \beta \leq \pi$

5. Cone (no bottom)

$$\sigma = \frac{2a\pi r^2}{\sin \phi} (\sin^2 \beta \cos^2 \phi + 2 \cos^2 \beta \sin^2 \phi \qquad 0 \leq \beta \leq \phi$$

$$= \frac{a\pi r^2}{\sin \phi} \left(1 + \frac{2}{\pi} \sin^{-1} \frac{\tan \phi}{\tan \beta}\right)(\sin^2 \beta \cos^2 \phi + 2 \cos^2 \beta \sin^2 \phi) +$$

$$\frac{6\pi a r^2}{\pi} \cos \beta \sqrt{\cos^2 \phi \sin^2 \beta - \sin^2 \phi \cos^2 \beta} \qquad \phi \leq \beta \leq 180 - \phi$$

r = radius
A = area (of flat plate)
ℓ = length (of cylinder)
ϕ = half angle of cone
β = angle of incidence

Various sorts of bodies can be conceived of as being made up of these basic configurations. For example, a complete hemisphere can be thought of as a hemisphere with no bottom (Eq. 4) plus a circular flat plate (Eq. 2) of area πr^2 and the cross-section of the sum is the sum of the cross-sections.

Figure 1 shows a polar plot of the cross-section for a complete hemisphere. Figure 2 shows the cross-section for a complete cylinder having various aspect ratios. Figures 3 and 4 show the relative sizes of cylinders and cones. Polar plots of the cross-section of cones with bases are shown in Figures 5 through 9 for various size half angles. Note that the cone indicates direction only; not relative shape.

4.2 Optical Cross-Section (Experimental)

Since the surface materials of vehicles which might be tracked by optical radar will not be either perfect diffuse reflectors or perfect specular reflectors,

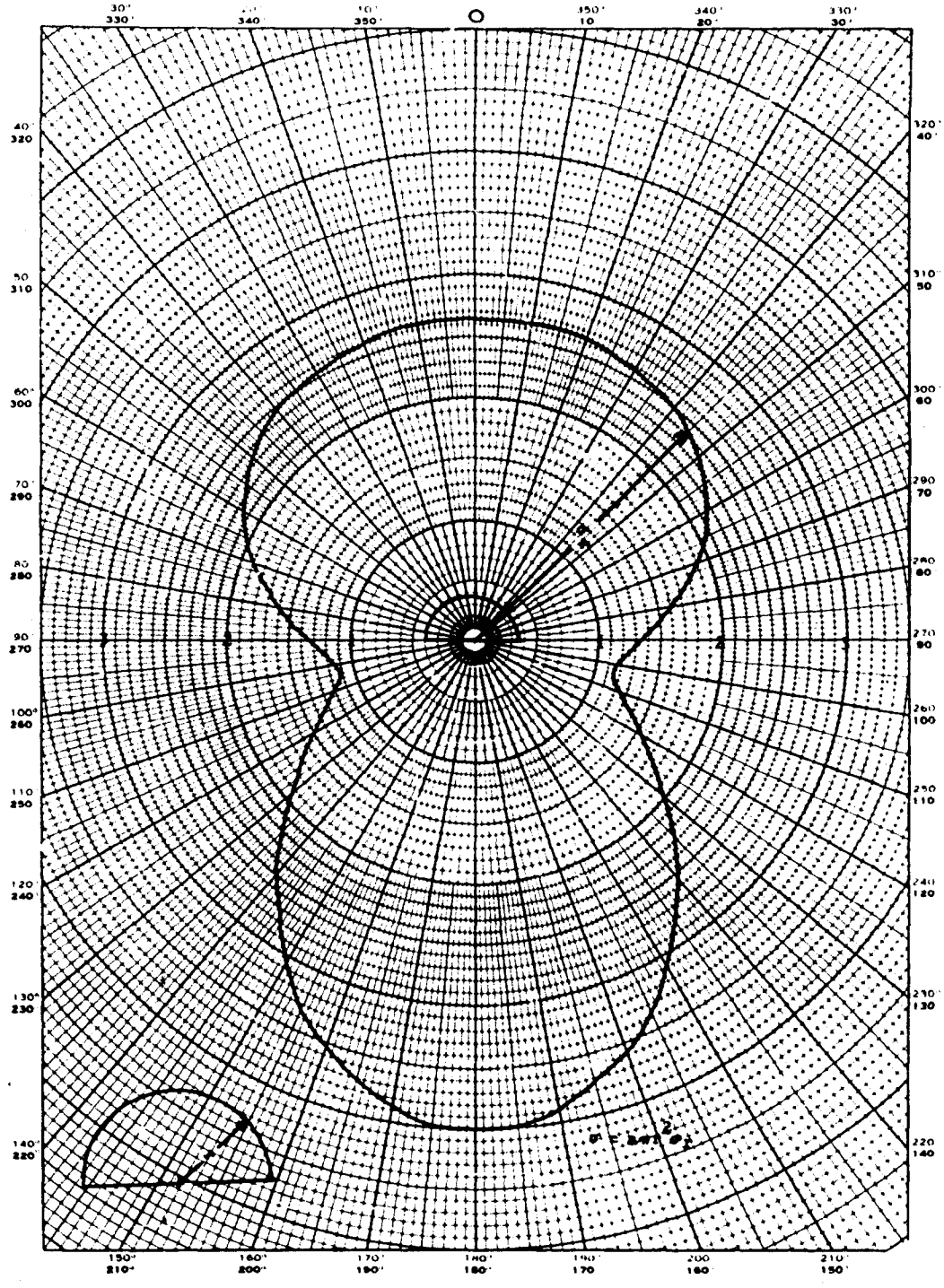

Figure 1. Polar Plot of Calculated Values for the Cross-Section of a Complete Diffuse Hemisphere.

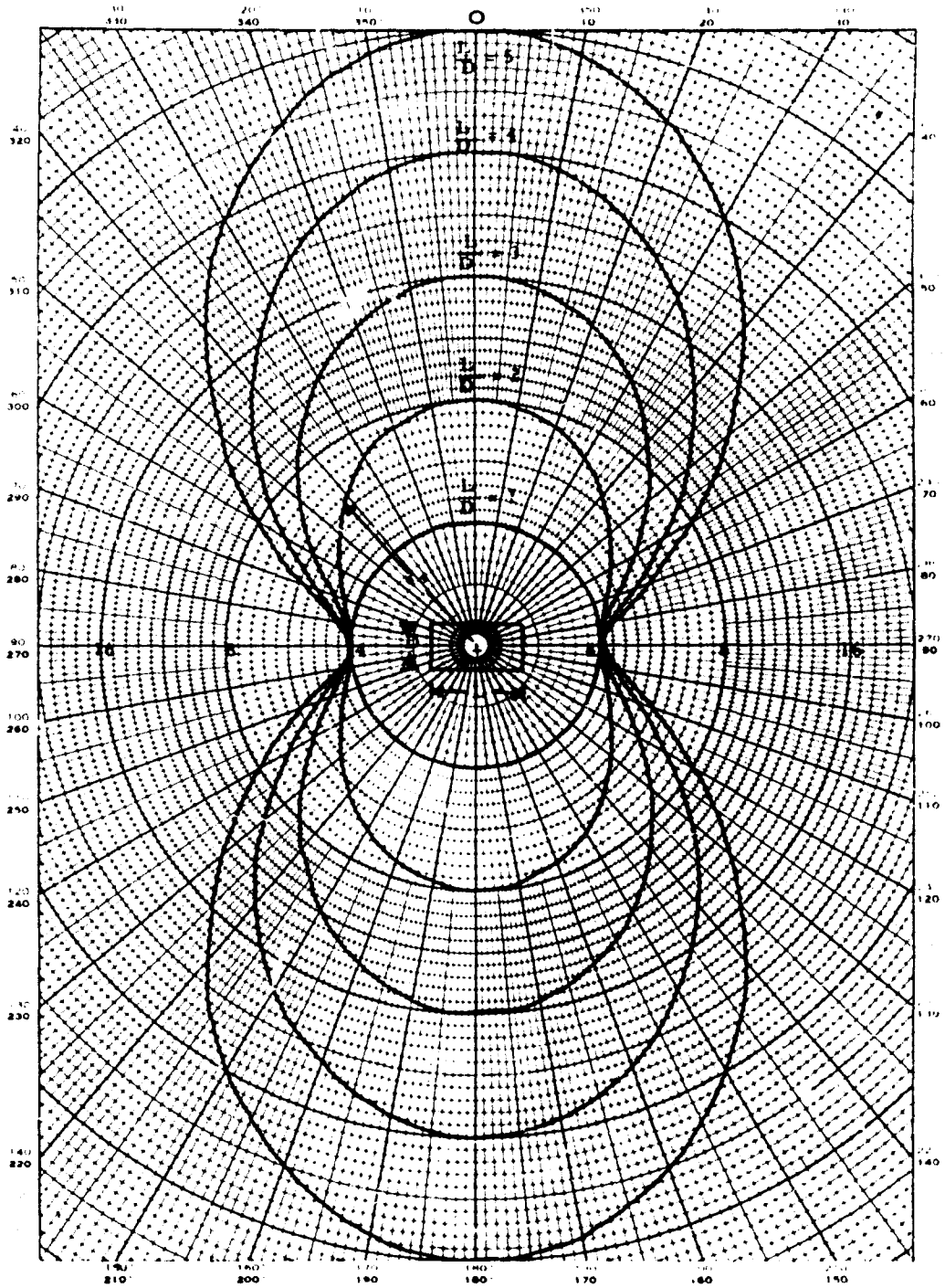

Figure 2. Polar Plot of Calculated Values for the Cross-Section of Cylinders of Various Sizes.

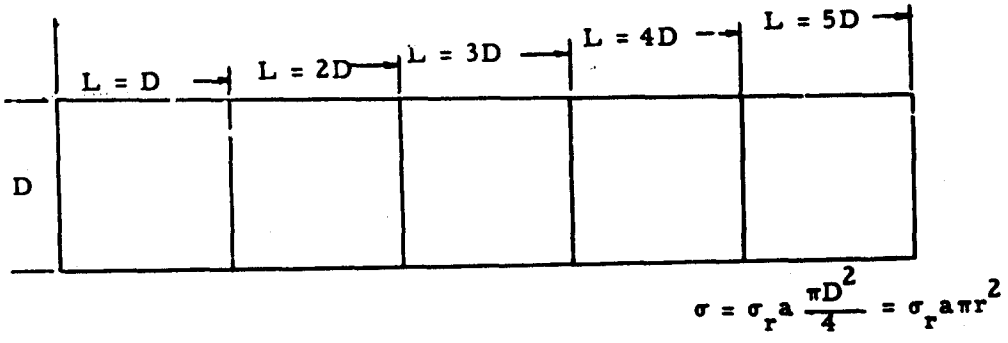

Figure 3. Relative Size of Cylinders

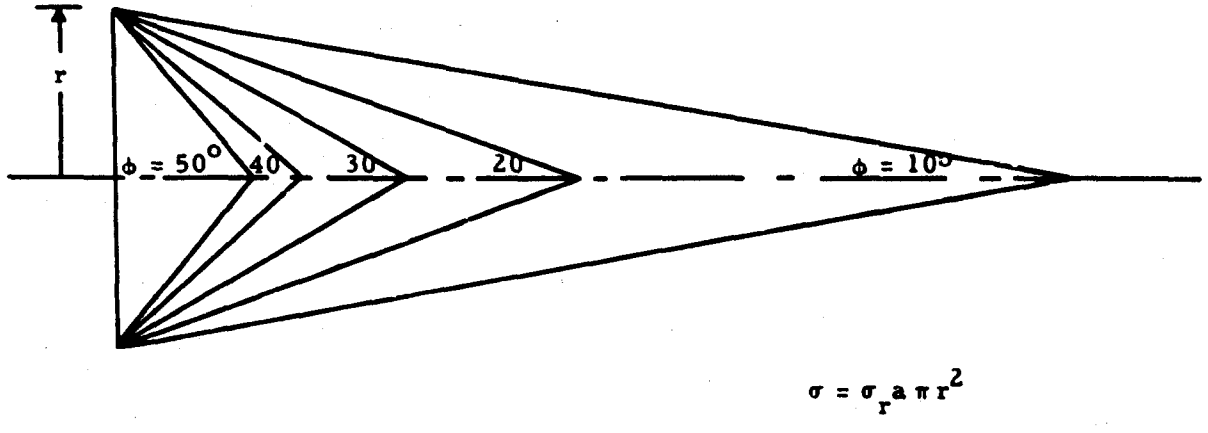

Figure 4. Relative Sizes of Cones

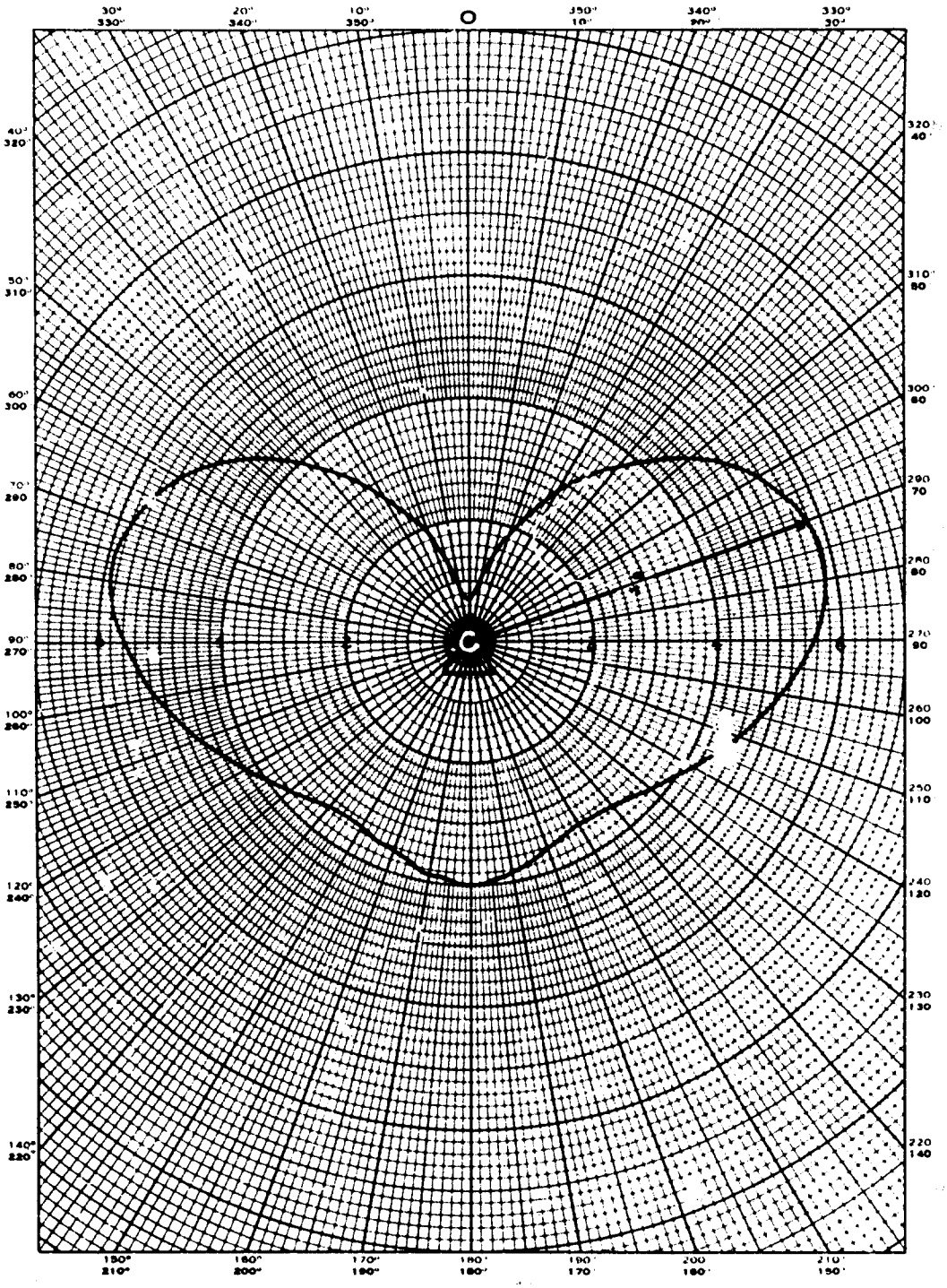

Figure 5. Polar Plot of Calculated Values for the Cross-Section of a Cone With 10° Half Angle.

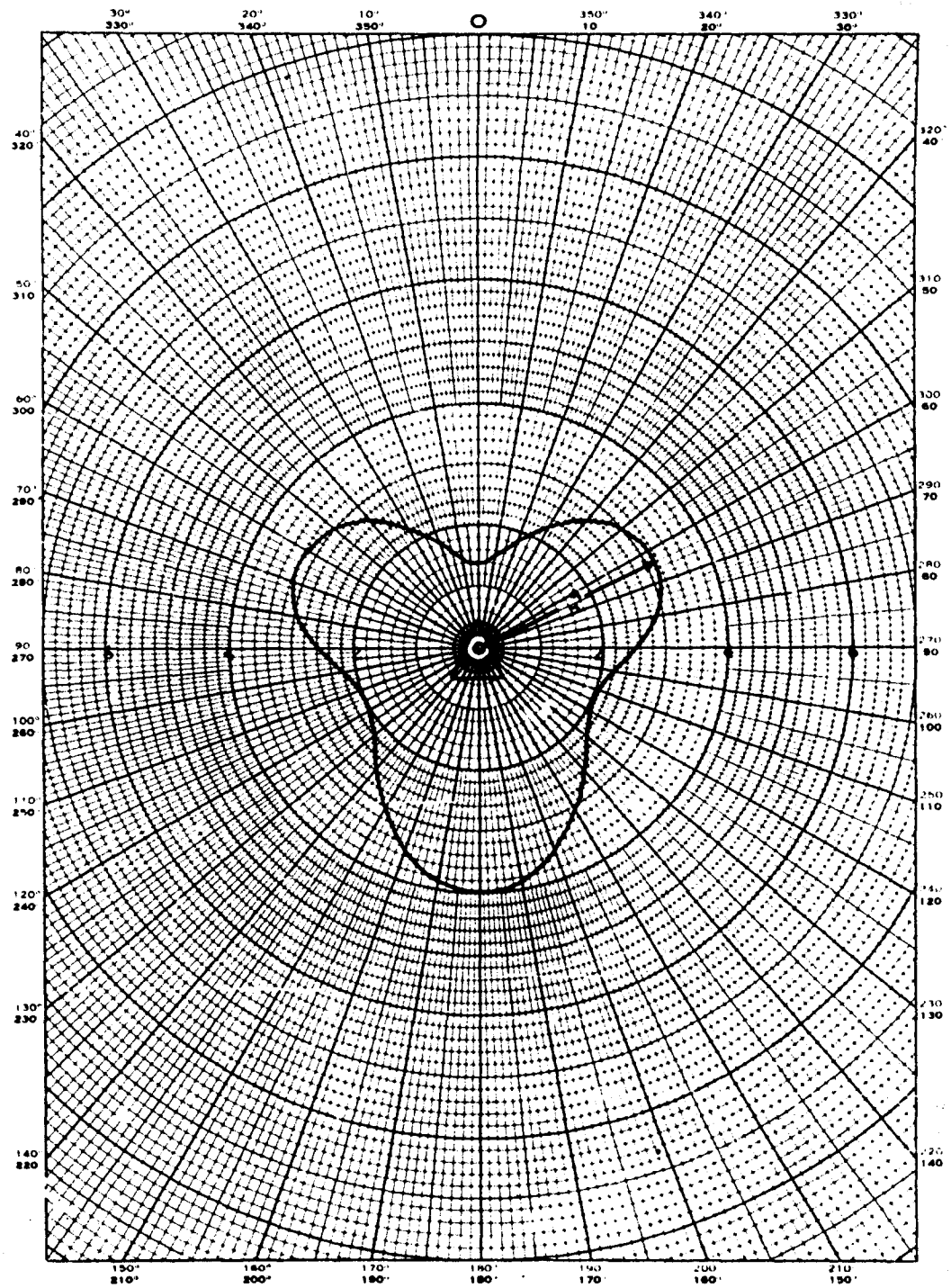

Figure 6. Polar Plot of Calculated Values for the Cross-Section of a Cone With 20° Half Angle.

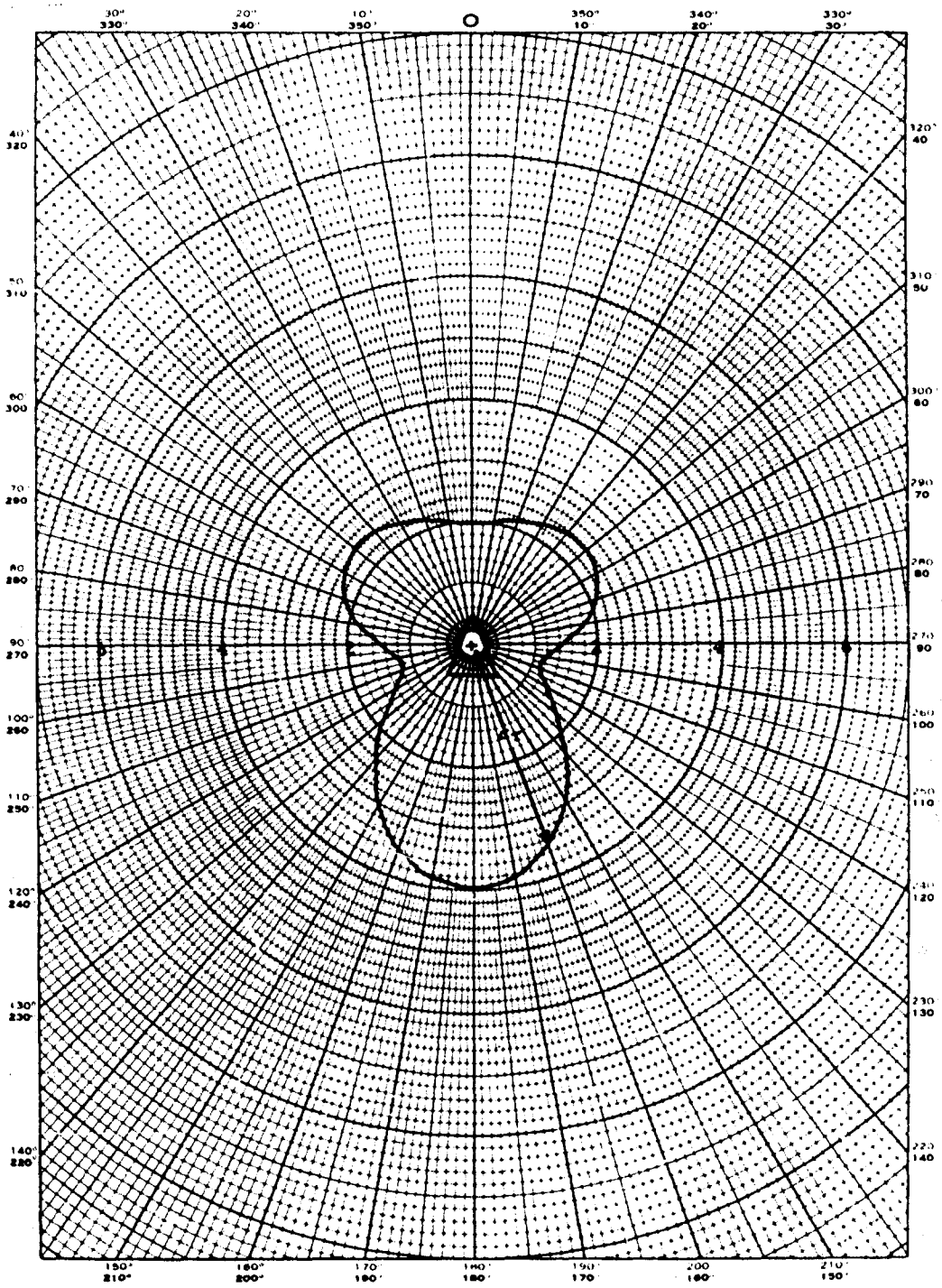

Figure 7. Polar Plot of Calculated Values for the Cross-Section of a Cone With 30° Half Angle.

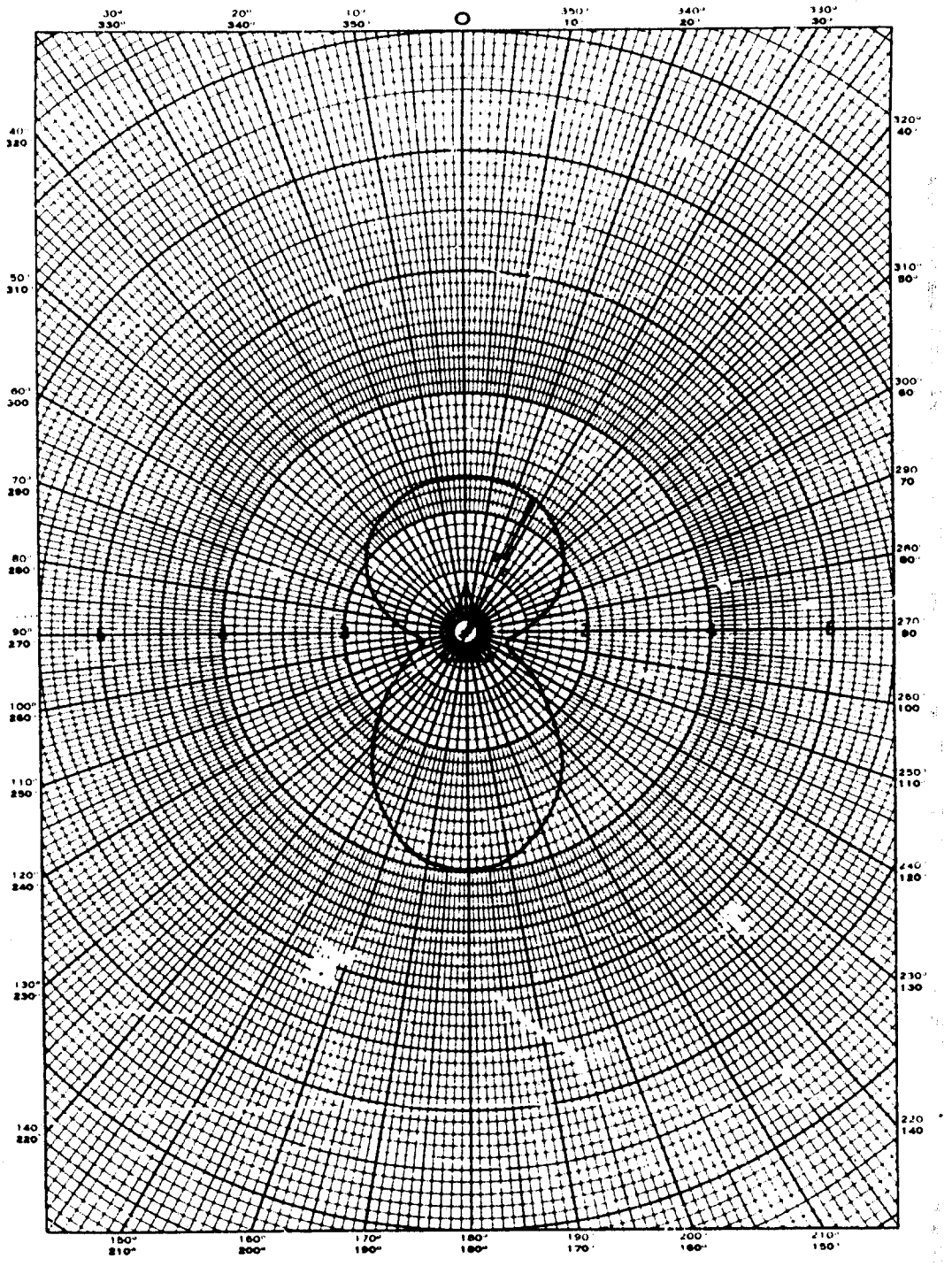

Figure 8. Polar Plot of Calculated Values for the Cross-Section of a Cone With 40° Half Angle.

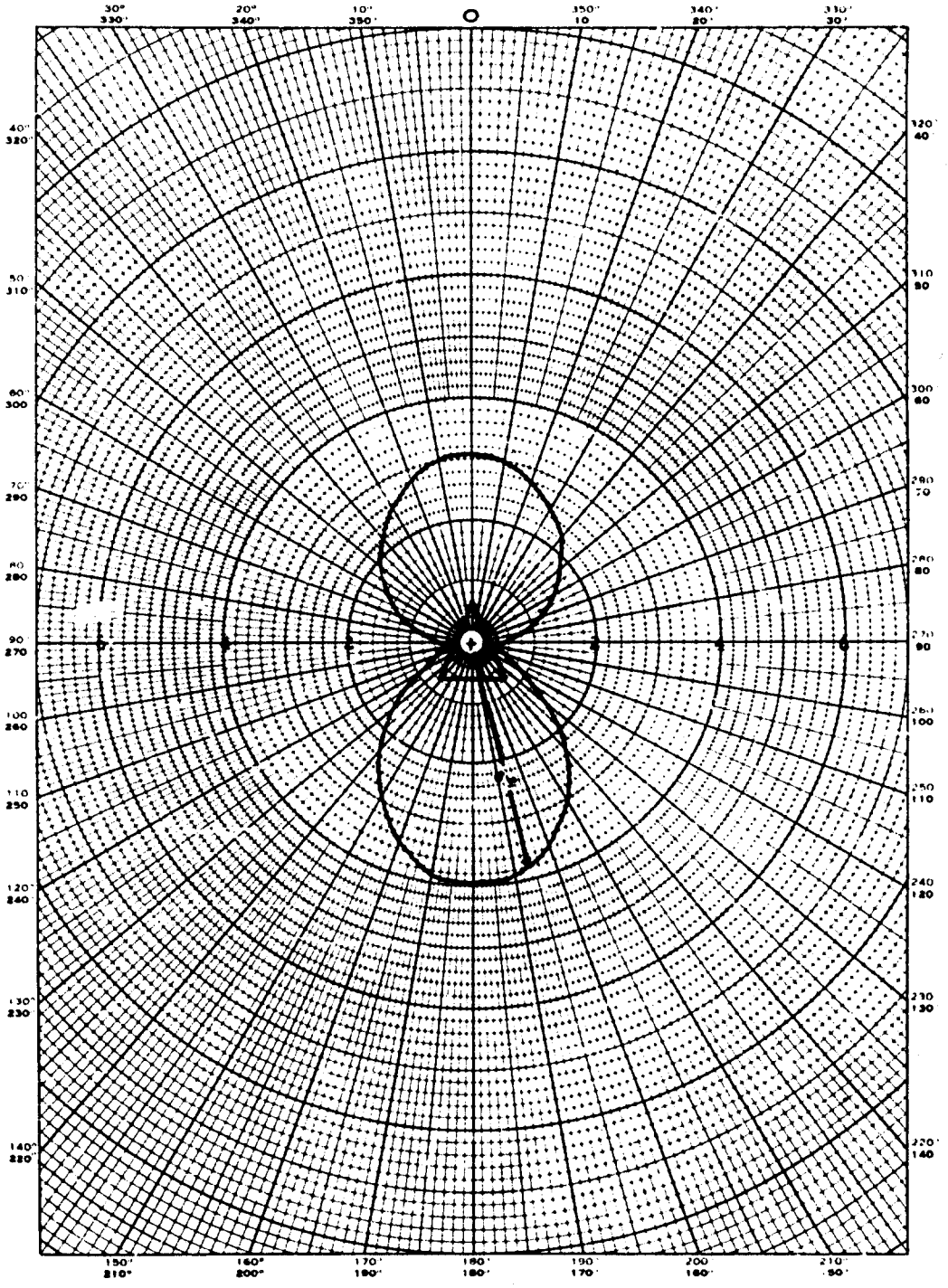

Figure 9. Polar Plot of Calculated Values for the Cross-Section of a Cone With 50° Half Angle.

the calculations in the foregoing section are in many ways unrealistic. It therefore was desirable to proceed experimentally in two directions: A) to determine the reflection coefficient for actual materials which might be used, and B) to determine the optical cross-section for models similar in both material and configuration to bodies of interest.

4.2.1 Reflected Light Distribution

The first of these investigations consists of measuring the ratio of the light reflected by a plane plate in any given direction (θ) to the light incident at any angle (ϕ). These data, in numerical form, could then be used to compute the optical cross-section for a body by numerical integration over the surface.

The schematic of the instrument developed is shown in Figure 10. The reflection coefficient for a diffuse reflecting body which obeys Lambert's Law can be defined as

$$a(\phi, \theta) = \frac{\pi r^2}{A} \frac{F_r}{F_i} \sec \theta$$

where

F_i = incident luminous flux per unit area, lumen-sec
F_r = reflected luminous flux per unit area, at range r, lumen-sec
r = radius of the device
A = area of entrance aperture

A modified x-ray diffraction device (see Figure 11) used in the experiment consists of a port (through which collimated external light enters), a film holder, and a sample holder free to rotate in a horizontal plane. A calibrated circle on the instrument designates the angular position of the sample. A photographic film is placed radially about the sample axis and equidistant from it, and the film surface is held parallel to the vertical axis of the sample surface. Thus, light reflected from the sample surface strikes the film surface normally.

The incident flux F_i is $F_o t$ (where F_o is the flux outside the instrument and t is the transmissivity of the glass plate). This is measured by the amount reflected from the glass plate ρF_o (where ρ is reflectivity of the glass plate). The flux then passes through the attenuator with transmissivity t_a and is incident on the film at an angle α. Hence, the total exposure on the film results from the flux $F_o \rho t_a \cos \alpha$. The equation for reflectivity then becomes

$$a(\phi, \theta) = \frac{\pi r^2}{A} \frac{F_r}{F_o t} \sec \theta = \frac{\pi r^2}{A} \frac{\rho t_a}{t} \frac{(F_r)}{(F_o \rho t_a \cos \alpha)} \cos \alpha \sec \theta$$

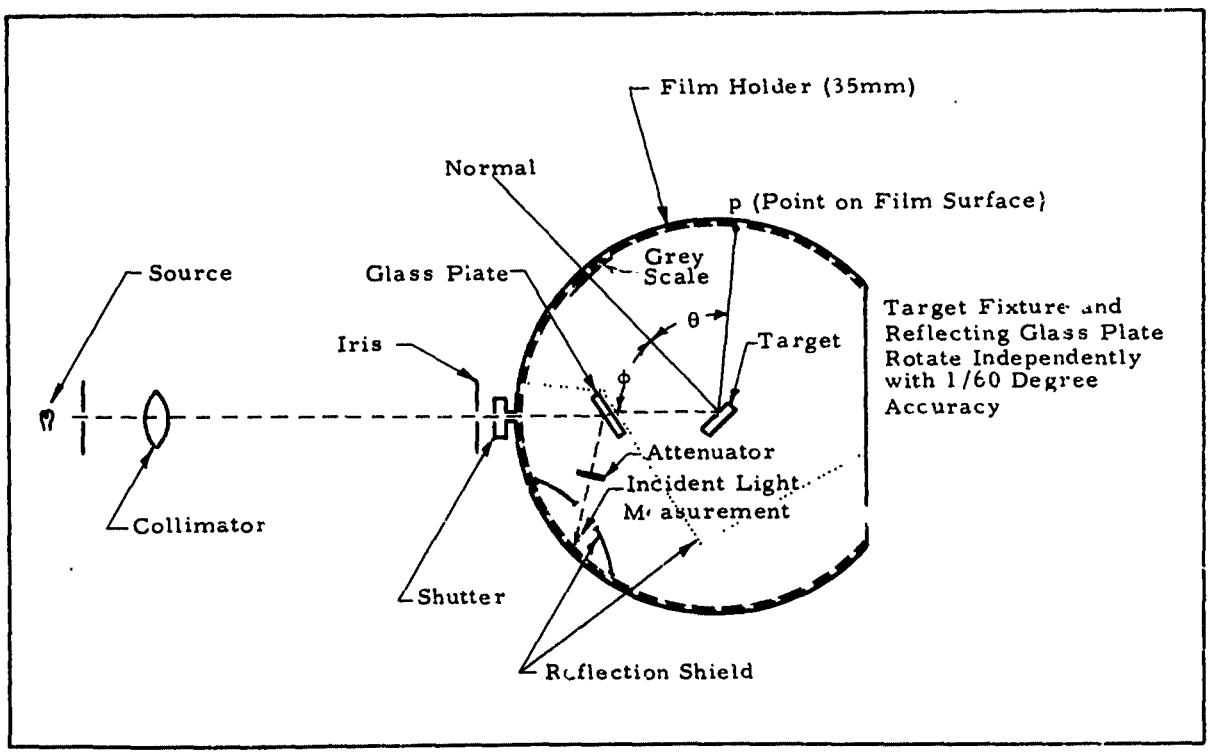

Figure 10. Schematic for Target Reflected Light Distribution Recording Device.

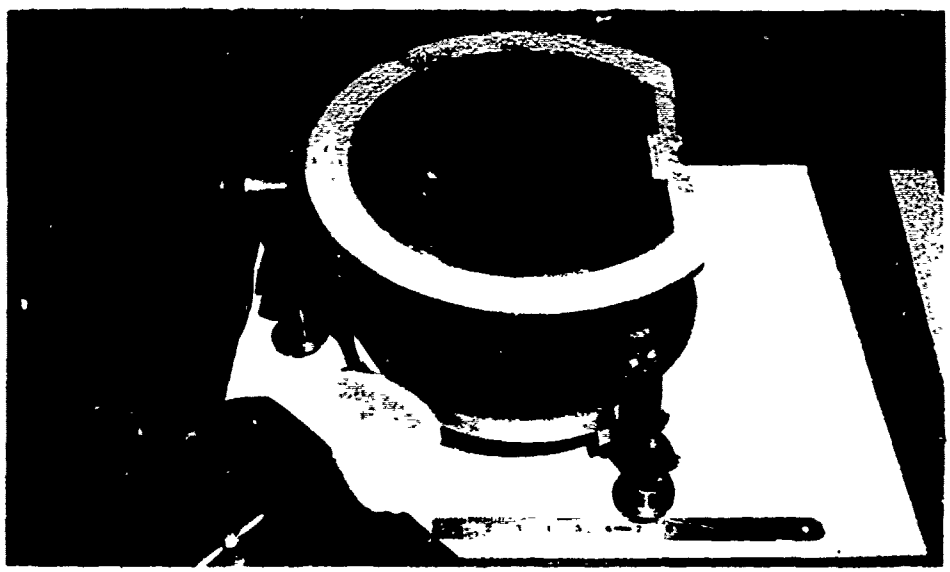

Figure 11. Photograph of Modified X-ray Diffraction Device Used for Light Distribution Recording Device.

The quantities in parentheses are the fluxes incident on the film and are measured by the exposures (lumen-sec) E_r and E_o. Thus

$$a(\phi,\theta) = \rho \frac{\pi r^2}{A} \frac{t_a}{t} \frac{E_r}{E_o} \cos\alpha \sec\theta$$

The exposure of the film is measured by the optical density of the film; however, optical density is not directly proportional to the exposure, but depends on the gamma curve for the film. This curve was obtained by the following procedure. After placing the film in the film holder of the apparatus, a calibrated step wedge (Kodak) was placed in front of the film, and at a position where the test surface normal intersected. The wedge was placed at this position since the illumination from the surface is approximately constant over this region. A collimated beam of light was allowed to enter the apparatus and reflect from the test surface for a specified exposure time (3, 5, or 7 minutes). Light which reflected from the surface passed through the step wedge to the film emulsion. The extent of the darking (density) was a function of the transmission of the wedge. The illumination incident upon the film was a function only of the transmission of the wedge since the illumination which struck the wedge was constant over the step wedge region. Therefore, when the transmission values of the step wedge were plotted against the film density values, the necessary calibration (the gamma curve) resulted. Although the densities were plotted against transmission, they are really percentages of the illumination, and hence are relative values. This is of little consequence since the exposures are used as a ratio and hence cancel out.

The instrument used for reading the film densities (Microdensitometer) was actually designed to give only relative densities, but absolute densities were likewise required in the experiment. Therefore, a standard step wedge (within the range of required densities) was used. The film densities were recorded on the same graph with the densities of the step wedge and absolute values were obtained by interpolation between the steps immediately above and below the point desired.

Various problems of internal reflection in the recording instrument had to be solved. Even though the interior of the diffraction apparatus was covered with black velvet type paper, abrupt density changes were apparent on the film. Elimination of the problem was achieved by correcting the interior surfaces of the instrument. The position of the abrupt density change gave some indication of the sources of

light reflection. Three sources were determined and eliminated: (1) reflections occurred from the attenuator used in filtering the spot ($F_o \rho t_a$) which served as a reference density; (2) reflections occurred between the 35 mm film and the film holder (even though the holder was painted dull black); (3) multiple reflections occurred between the step wedge and the film because the film was not flush with the wedge.

Resulting data are shown in Figure 12. This is a plot of the density distribution on one film sample. The target used was a flat diffuse surface. Figure 13 is a plot of $a(\theta, \phi)$ as a function of θ for various angles ϕ. Departures from that expected for a pure Lambertian surface result from the specular characteristics of the sample. Further analysis of this data will be carried out at a later time, as well as exposure of varied samples.

4.2.2 Direct Cross-Section Photometry

The second of the methods used consists of measuring the ratio of the intensity of the light reflected back in the same direction as the incident light to the intensity of the incident light. This ratio is proportional to optical cross-section. A complete scaled model of the target was made for this measurement.

The schematic of the experimental set-up is shown in Figure 14. The entire arrangement is housed in a light-tight wooden box 3' x 8' x 18" high. Optical cross-section was defined in Section 4 of this report as $4\pi R^2$ times the light intensity reflected directly back to the light source divided by the intensity of light incident on the target in question. Because a Laser beam as a light source is quite narrow and the distances involved will be quite large, the beam incident on the target may be considered as parallel. Hence, for the purpose of simulation, a collimated light beam was used which enters the box from one side. The light source used is a 6 volt 48 watt incandescent bulb. The intensity of the beam (designated as F_o) is about 6 lumens per square foot. The exact value is immaterial since only relative values need to be known in this experiment. Of this intensity, a fraction $F_o \rho$ is reflected from the image divider and of this a fraction $F_o \rho t_a$ is incident on the photomultiplier P_1. The voltage output from the photomultiplier P_1 is then a measure of $F_o \rho t_a$. The image divider is kept to as small an angle of incidence as possible (approximately 7^o) so as to make the reflection factor r and the transmission factor t nearly independent of polarization. The attenuator at P_1 although it is shown normal to $F_o \rho$ is also placed at a slight angle so that the reflection from it does not

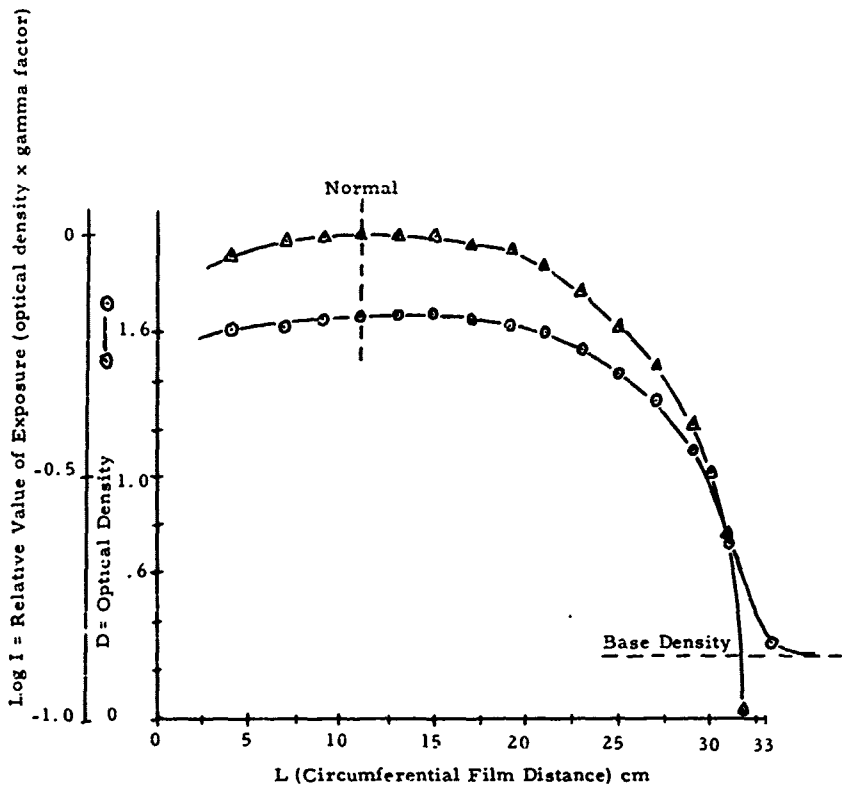

Figure 12. Optical Density Distribution on One Film Recorded in the Light Distribution Recording Device; the Target was a Flat Diffuse Surface

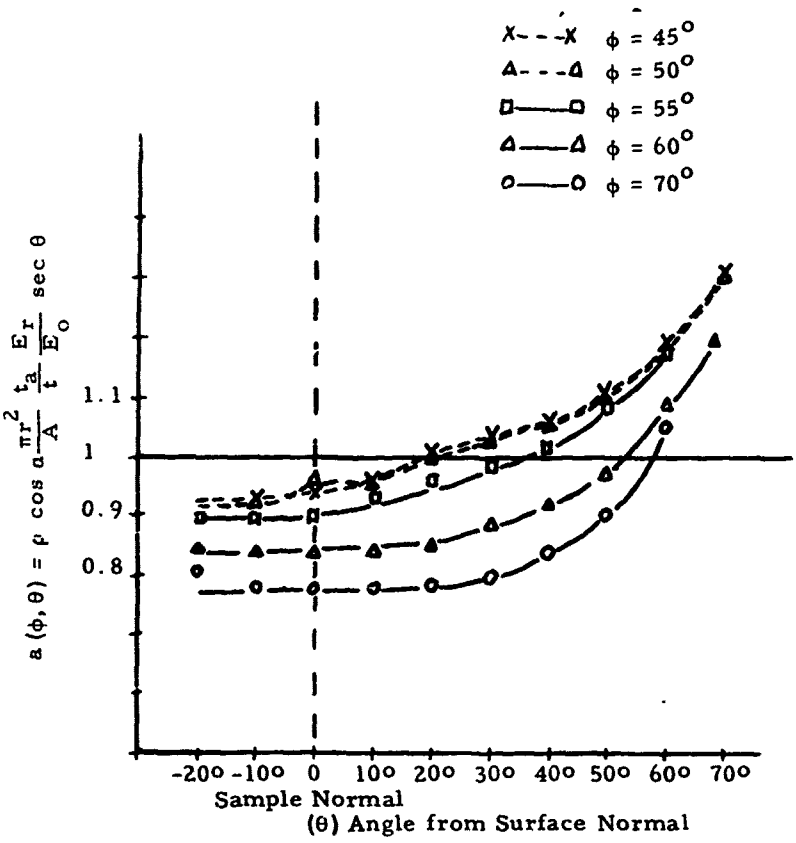

Figure 13. Reflection Coefficient, a (φ, θ), Shown as a Function of θ and for Various Angles φ. The Target Used was a Flat Diffuse Surface.

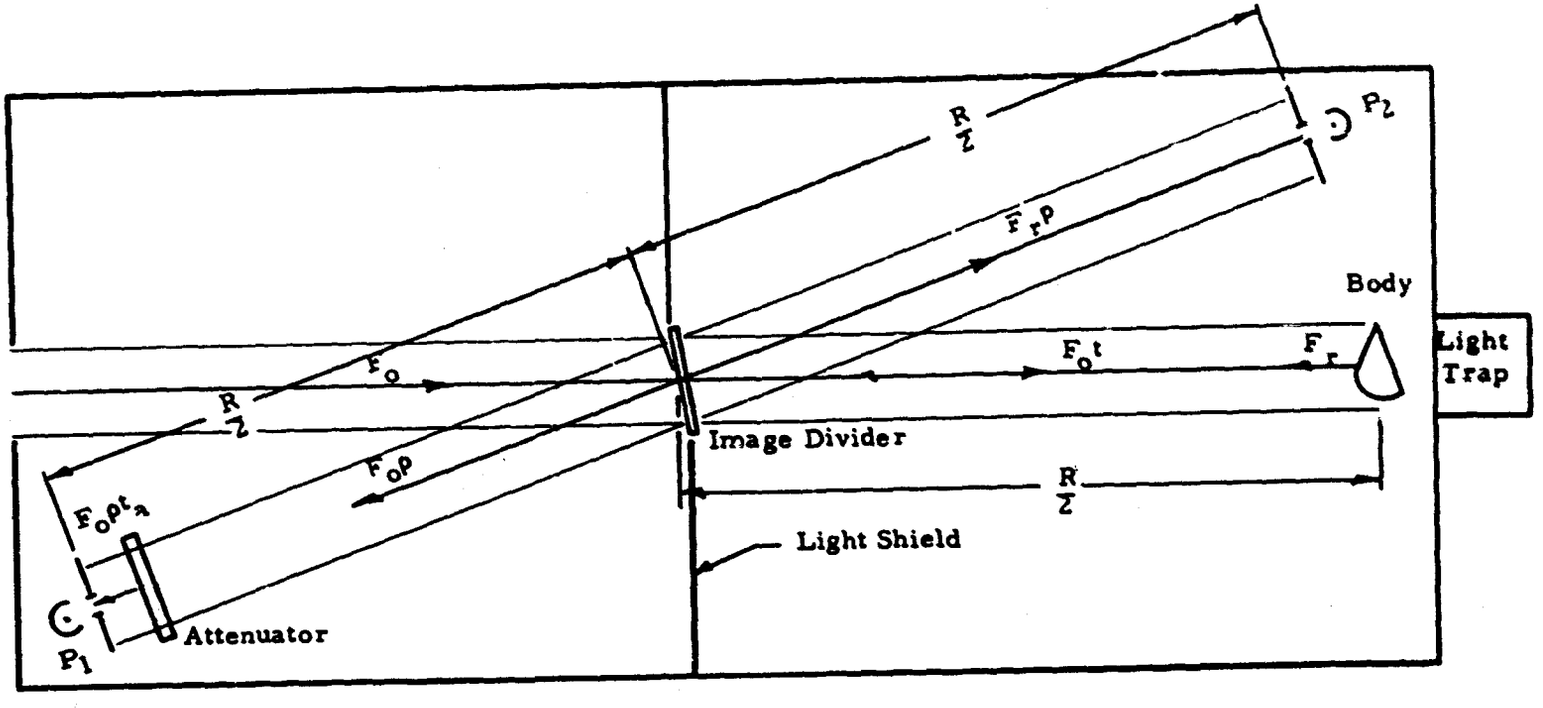

Figure 14. Schematic of Photometric Device Used for Cross-Section Measurements

fall on photomultiplier P_2. This attenuator serves the function of reducing the magnitude of the signal at P_1 to about the same magnitude as that at P_2.

The transmitted beam $F_o t$ then becomes the light incident on the test body for which the optical cross-section is desired. The test body and the photomultiplier P_1 are positioned at the same range $\frac{R}{2}$ from the divider to compensate for any possible divergence effect. The beam reflected directly back towards the source is likewise reflected from the image divider and has the intensity $F_r \rho$ at the photomultiplier P_2 at the total range R. The definition of optical cross-section σ becomes

$$\sigma = 4\pi R^2 \frac{F_r}{F_o t}$$

since the incident flux is $F_o t$ and the reflected flux at range R is F_r. Now multiplying both numerator and denominator by the factors ρ and t_a the working equation

$$\sigma = 4\pi R^2 \frac{t_a}{t} \frac{F_r \rho}{F_o \rho t_a} = 4\pi R^2 \frac{t_a}{t} \frac{p_2}{p_1}$$

is obtained, where p_1 is the light flux on photomultiplier number one ($F_o \rho t_a$) and p_2 is the light flux on photomultiplier number two. Both photomultipliers are calibrated to measure light intensity directly by using the same light source as will be discussed below.

The test body is mounted on a vertical shaft which rotates the body in a horizontal plane at a rate of one revolution per minute. The output of photomultiplier number two is fed into a D.C. amplifier where a bias (or bucking) voltage is generated in order to zero the output of the amplifier when the test body is taken out of the beam. The background results primarily from light scattered from the image divider and light which is scattered from the light-trap. The test body is then repositioned in the beam and the gain of the amplifier advanced until the output is on the order of 1 to 10 volts. The test body is again removed and the output is again biased to zero at the higher gain setting. This output of the D.C. amplifier is a known factor times the voltage (and hence intensity of light) from the photomultiplier. A schematic of this portion of the circuitry is shown in Figure 15.

The output of the amplifier is sent into an analog computer where it is multiplied by $\cos \omega t$. These functions which are generated by the computer are synchronized with the rotation of the test body, i.e., 2π radian/min. The output, $\sigma(t) \cos \omega t$ and $\sigma(t) \sin \omega t$ are plotted as the vertical and horizontal arms of an x-y

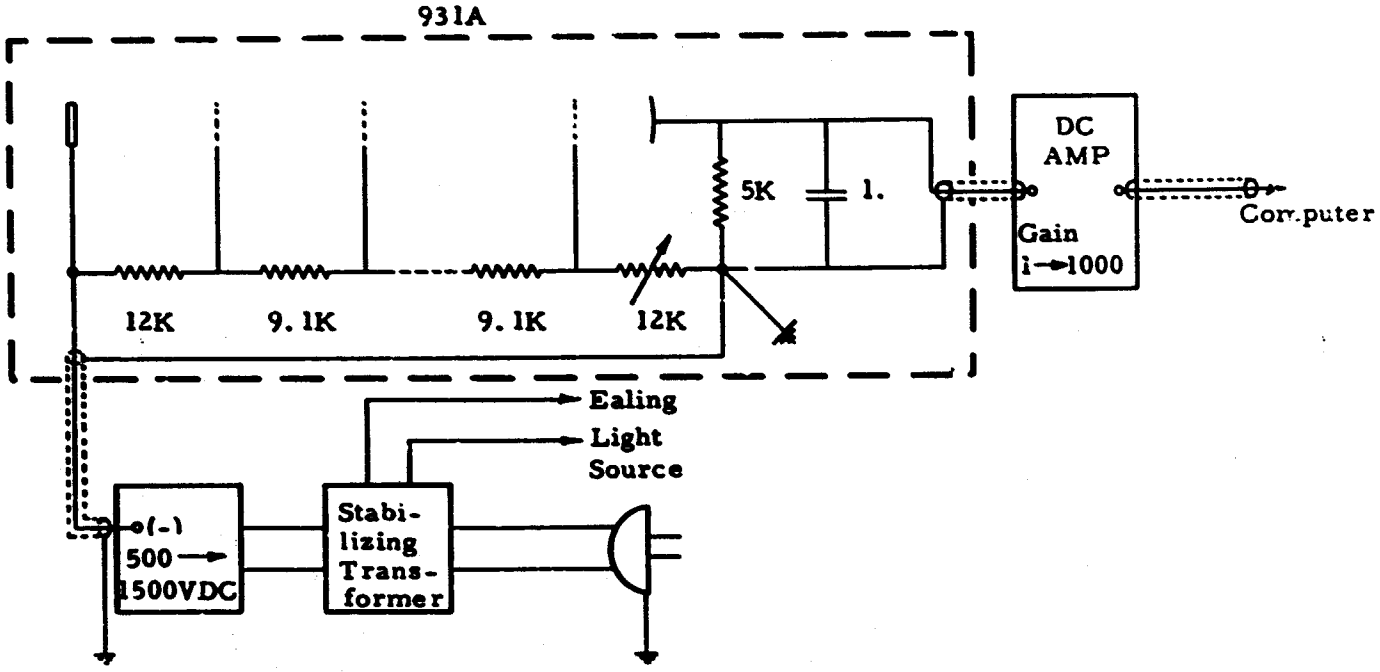

Figure 15. Photomultiplier Circuitry Used in Cross-Section Measurement Device.

plotter. Hence, the optical cross-section is plotted automatically in the form of a radius vector (polar plot) as a function of angle of rotation of the test body. The schematic of this circuitry is shown in Figure 16. Figures 17 and 18 are photographs showing the overall experimental set-up.

Up to this time, no attempt had been made to calibrate the system since it was first necessary to show that the system would work. The computer and x-y plotter, of course, required no calibration but were spot checked for accuracy. The gain of the D.C. amplifier was also checked by putting in known small voltages and plotting or measuring the output voltages. It was found to be quite reproducible but off by a factor 0.08 from the dial setting at all ranges.

Because of the difficulty of obtaining and reproducing a standard light source (particularly with the same spectral characteristics of the light used in this experiment) it was decided not to work with absolute light intensity levels but only with relative values a[illegible] near the intensity to be experienced in the experiment. It was therefore advisable to use the same light source as the experimental set-up and to use the inverse square (from a point source) as a means of obtaining relative values of light intensity. Distances on the order of 12 to 30 feet from the light source were used so that the source would appear as a point source and follow a true inverse square relationship. Neutral density filters were used with the inverse square relationship to regulate the light intensity. The output of one of the photomultipliers was balanced by a null galvanometer circuit with the voltage from a precision potentiometer. From these data it was possible to check the neutral density filters, to calibrate the photomultiplier and to compute the transmission of the attenuator (t_a) and the image divider (t). The response of the photomultiplier was found to be quite linear with light input. The second photomultiplier was calibrated by comparison to the first and was also found to be quite linear although it differed by a factor of about three from the first.

Since the output of photomultiplier number one is found to be quite constant during the time required for a cross-section polar plot, it is not necessary to form the quotient $\frac{p_2}{p_1(t)}$ but rather a factor $\frac{4\pi R^2 t_a}{t p_1}$ times $p_2(t)$ may be plotted. If R is in centimeters, the cross-section σ is in square centimeters. A number of simple models were fabricated from different materials in the form of small cones and cylinders. Figures 19 through 25 show tracings of the polar plots of the cross-section of a few representative bodies. The irregularities observable on some of

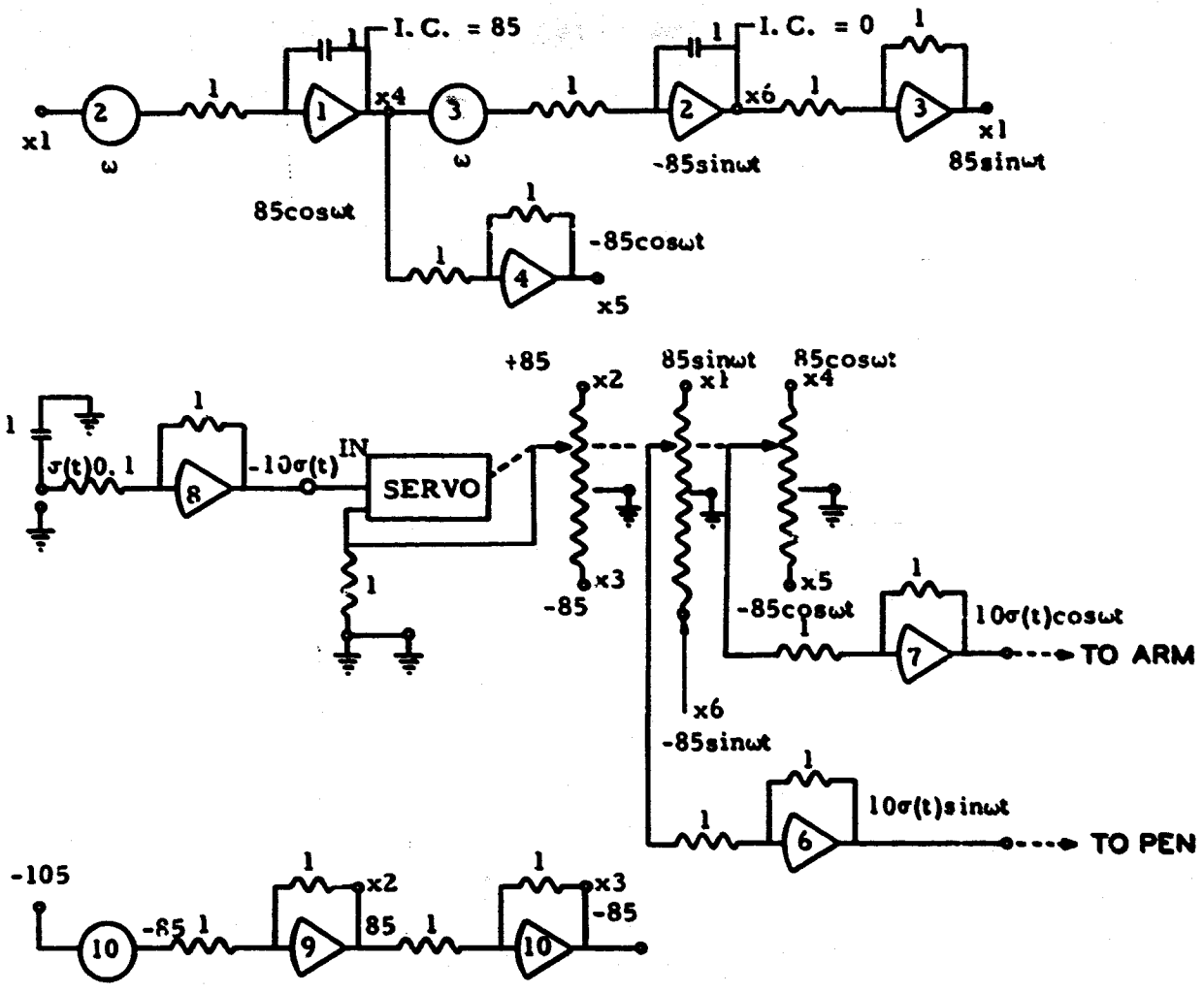

Figure 16. Analog Computer Circuitry Used in Cross-Section Measurement Device.

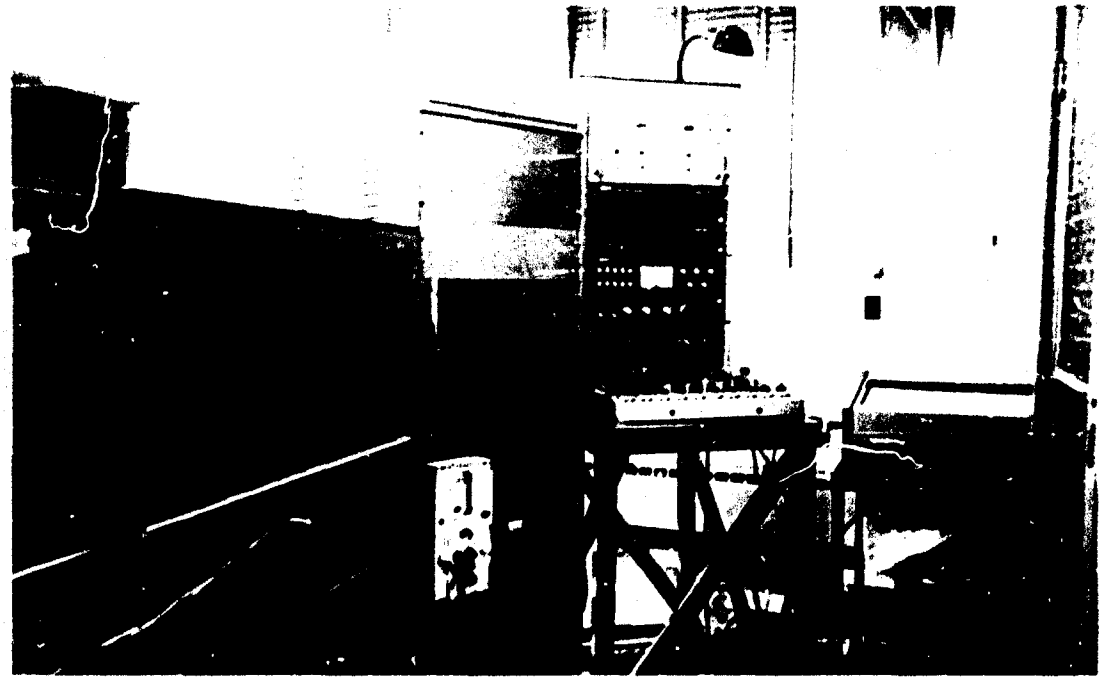

Figure 17. Photograph of Laboratory Set-up of Experimental Cross-Section Measurement Device (Front)

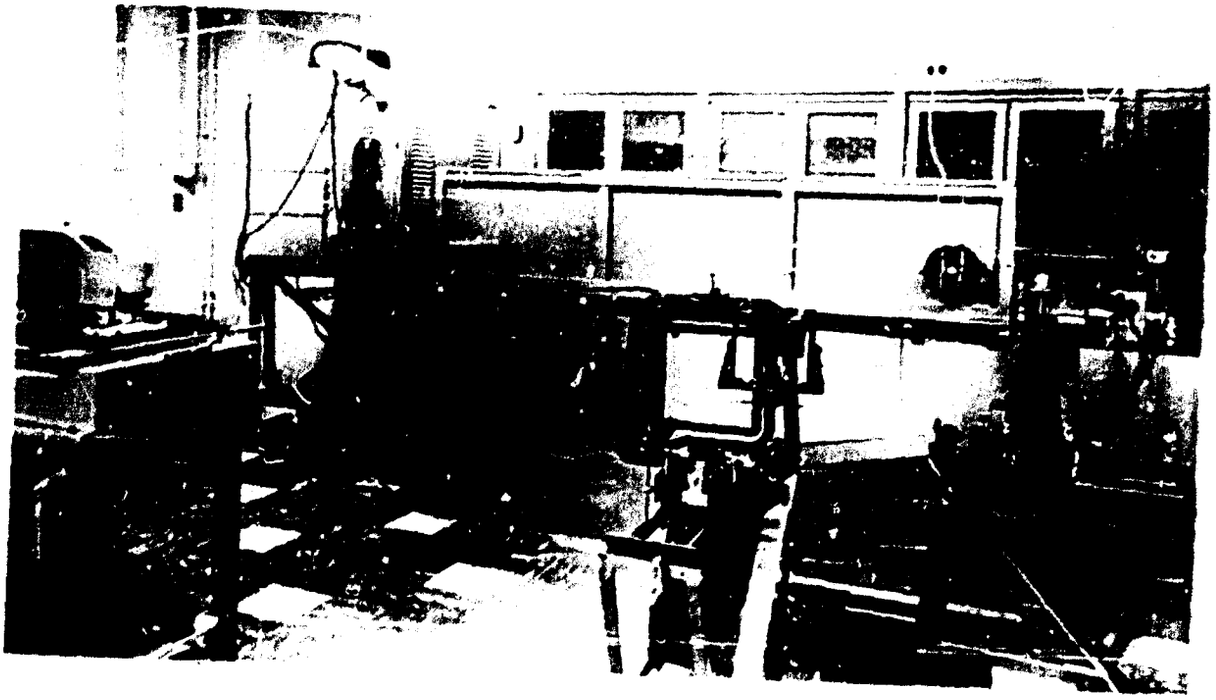

Figure 18. Photograph of Laboratory Set-up of Experimental Cross-Section Measurement Device. (Rear)

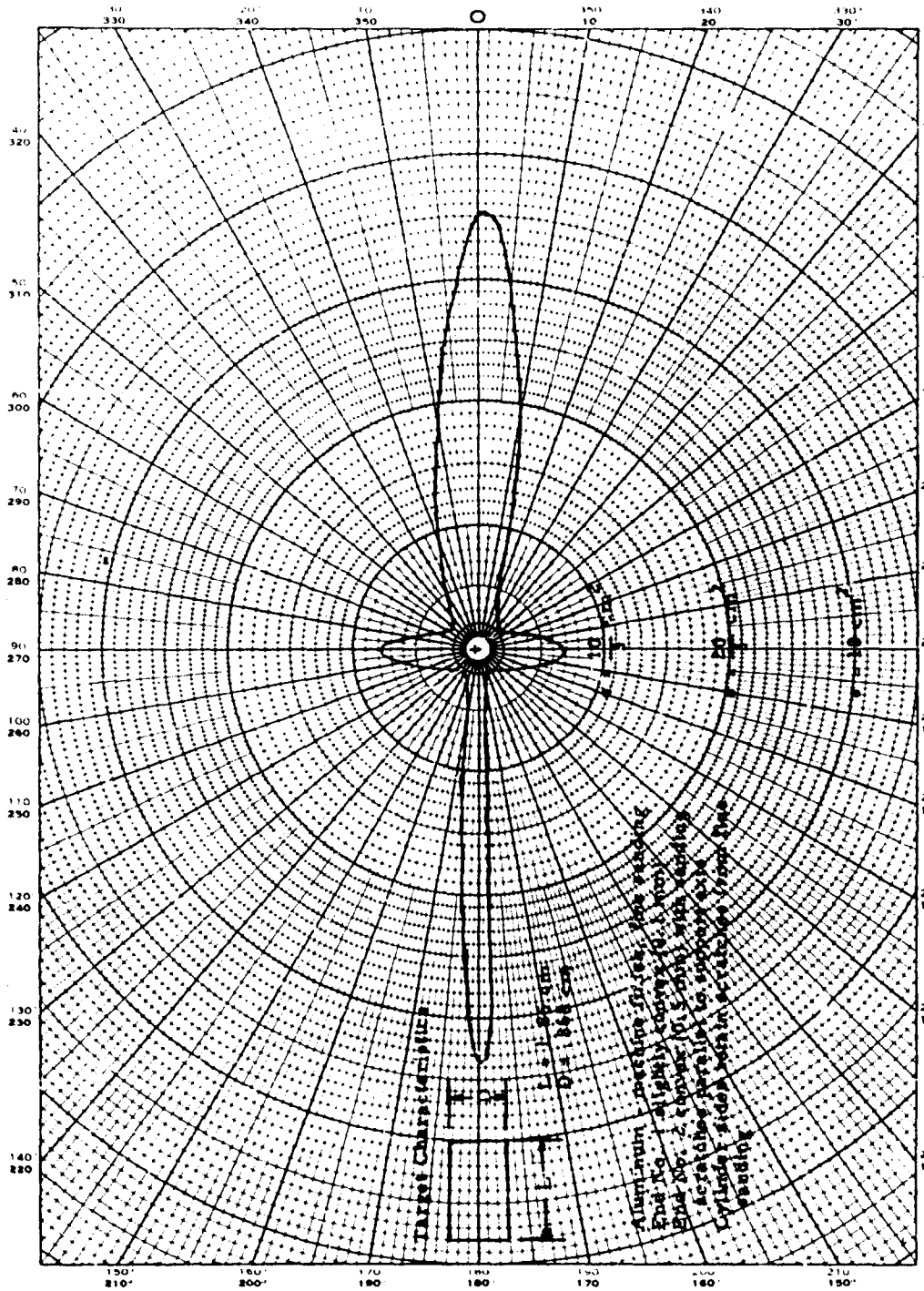

Figure 19. Polar Plot of Experimental Determination for Cross-Section Aluminum Cylinder.

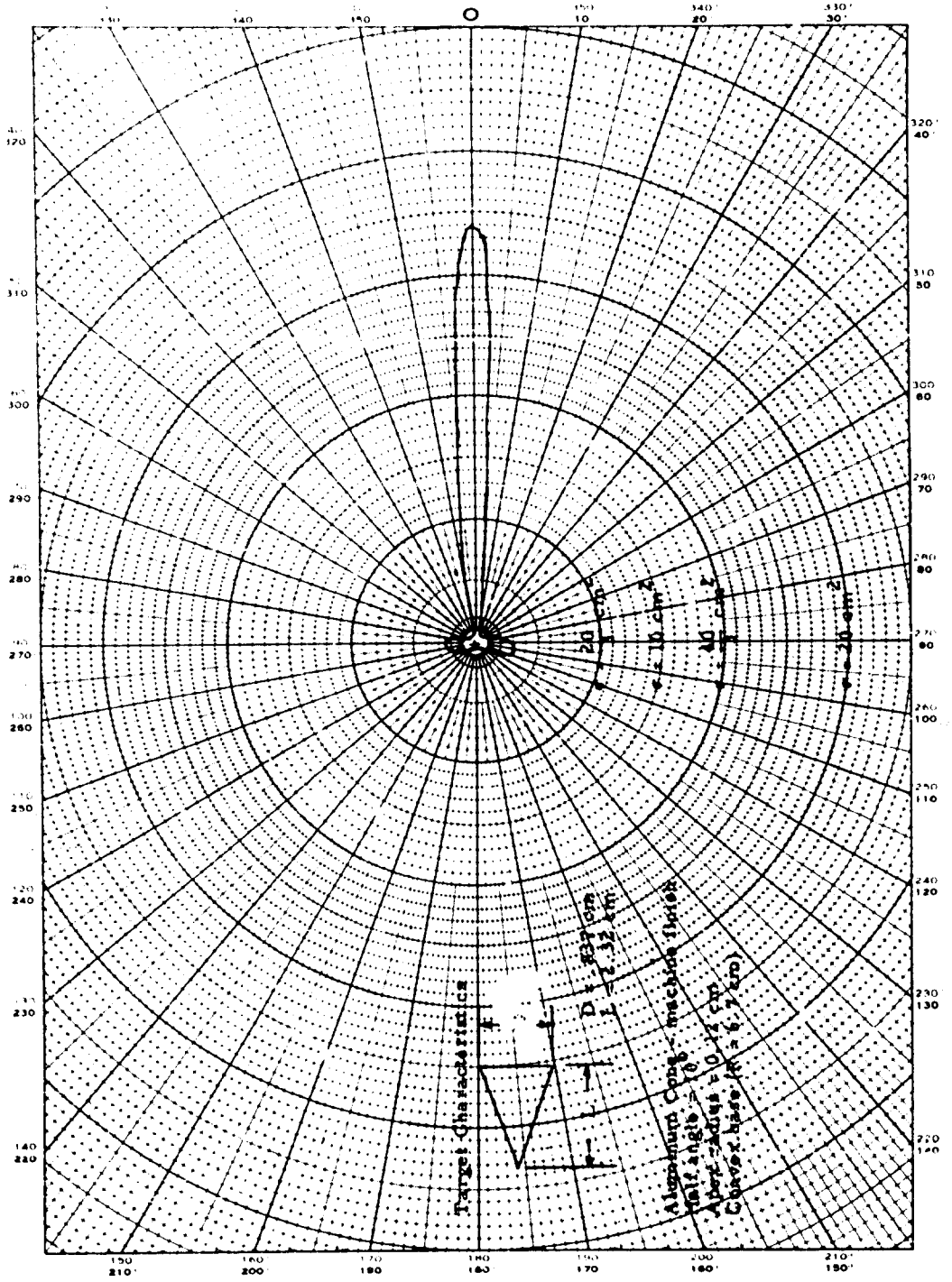

Figure 20. Polar Plot of Experimental Determination for Cross-Section of Aluminum Cone.

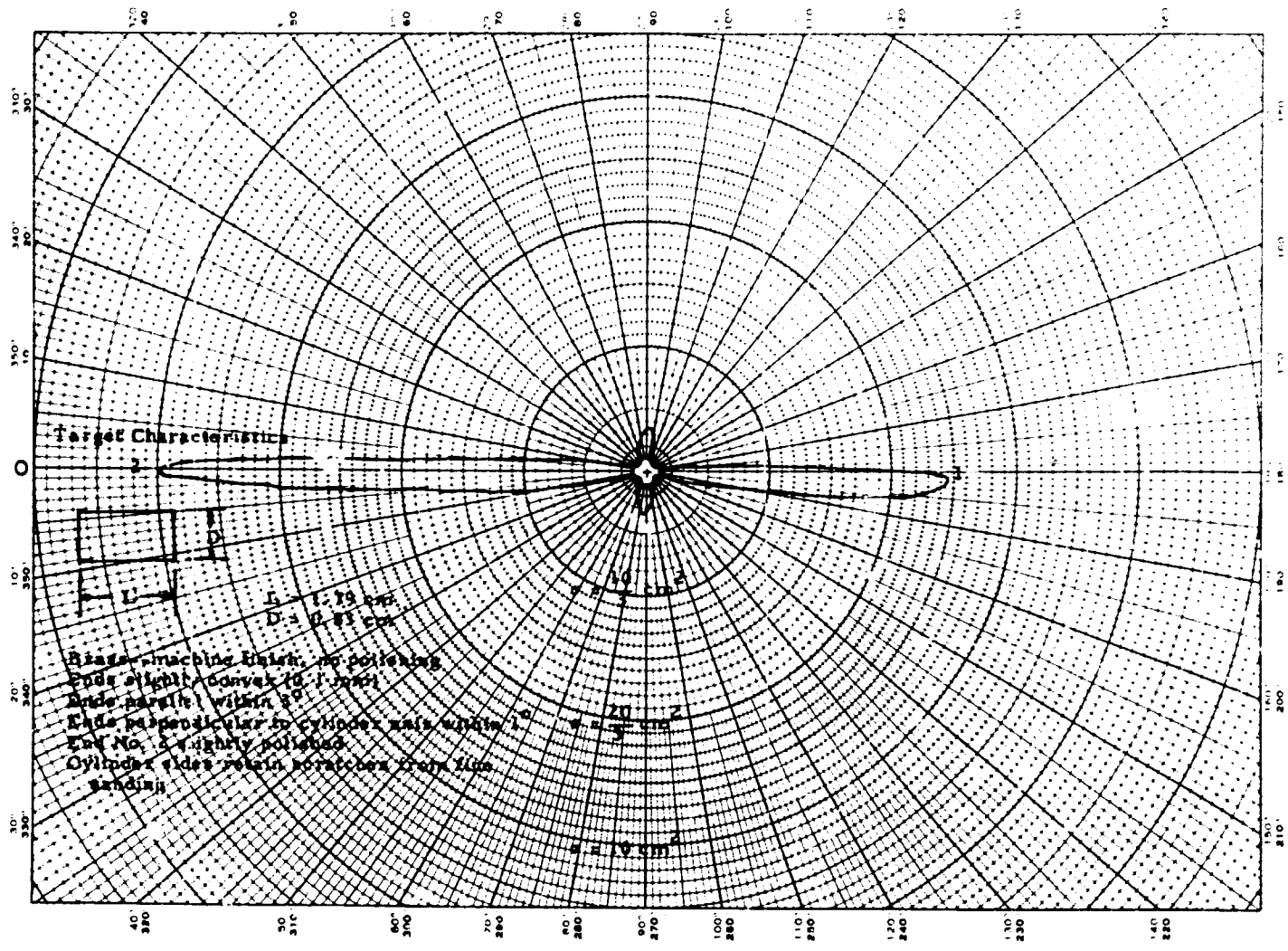

Figure 21. Polar Plot of Experimental Determination for Cross-Section of Brass Cylinder.

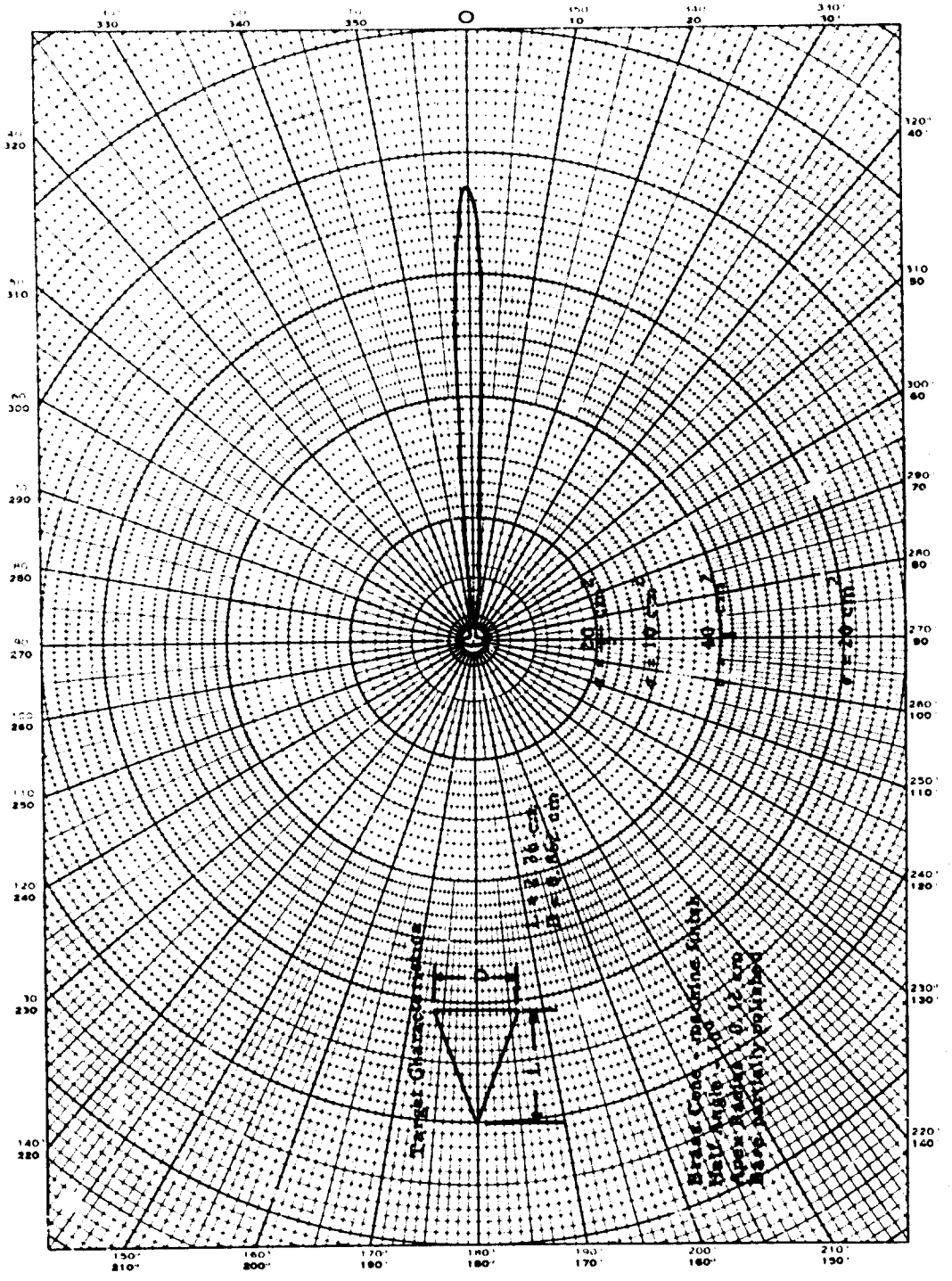

Figure 22. Polar Plot of Experimental Determination for Cross-Section of Brass Cone.

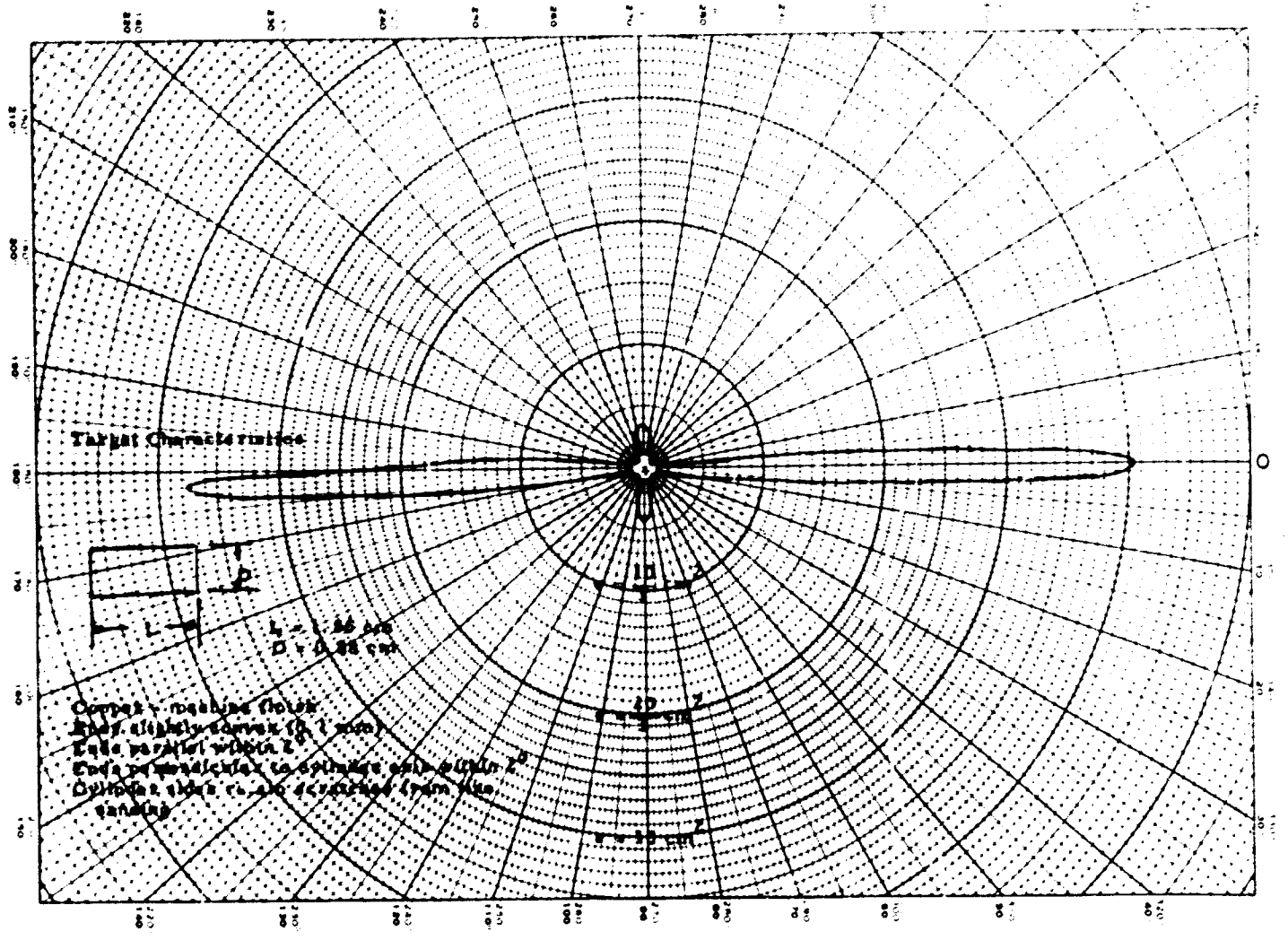

Figure 23. Polar Plot of Experimental Determination for Cross-Section of Copper Cylinder.

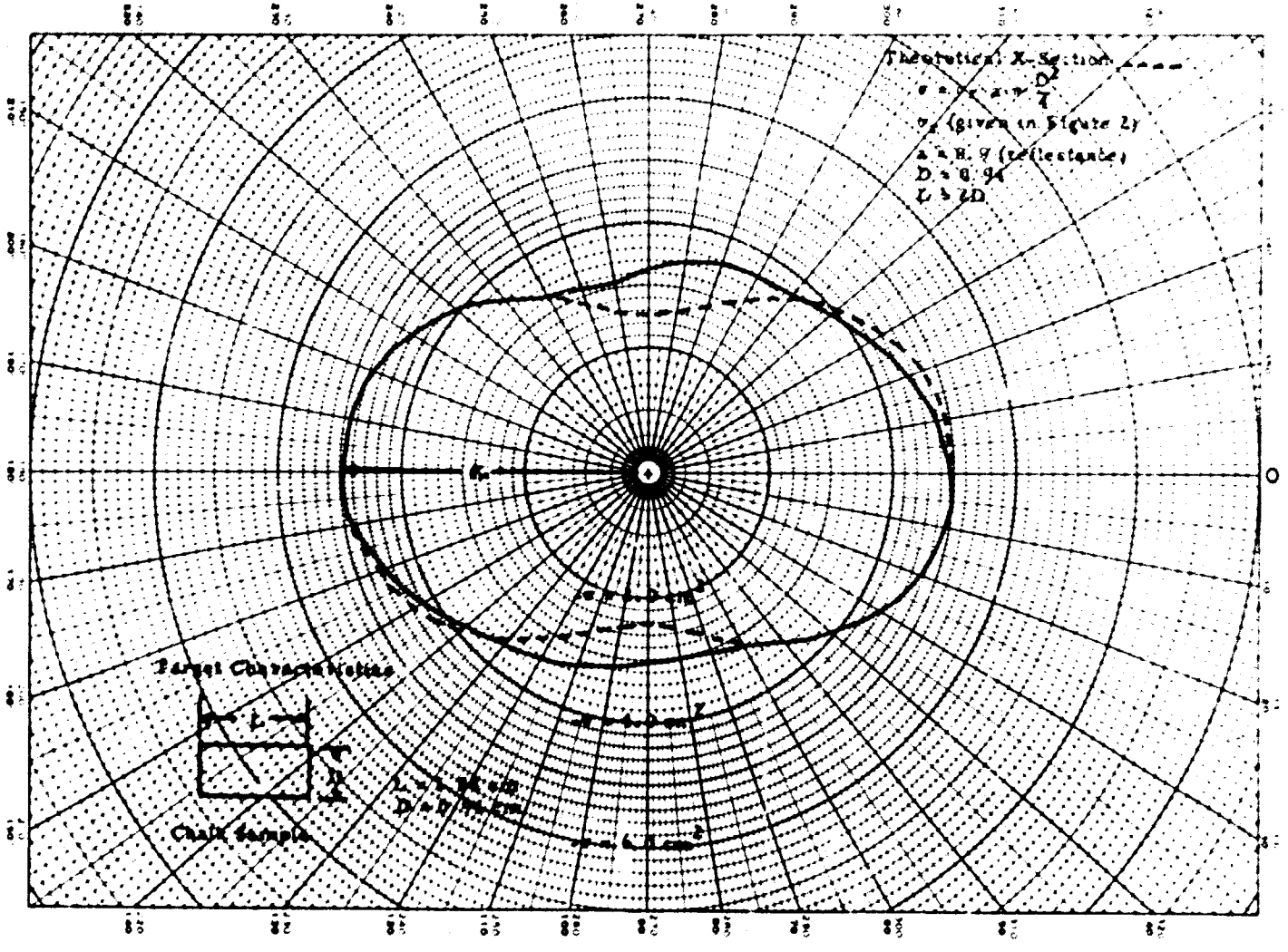

Figure 24. Polar Plot of Experimental Determination for Cross-Section of Chalk Cylinder.

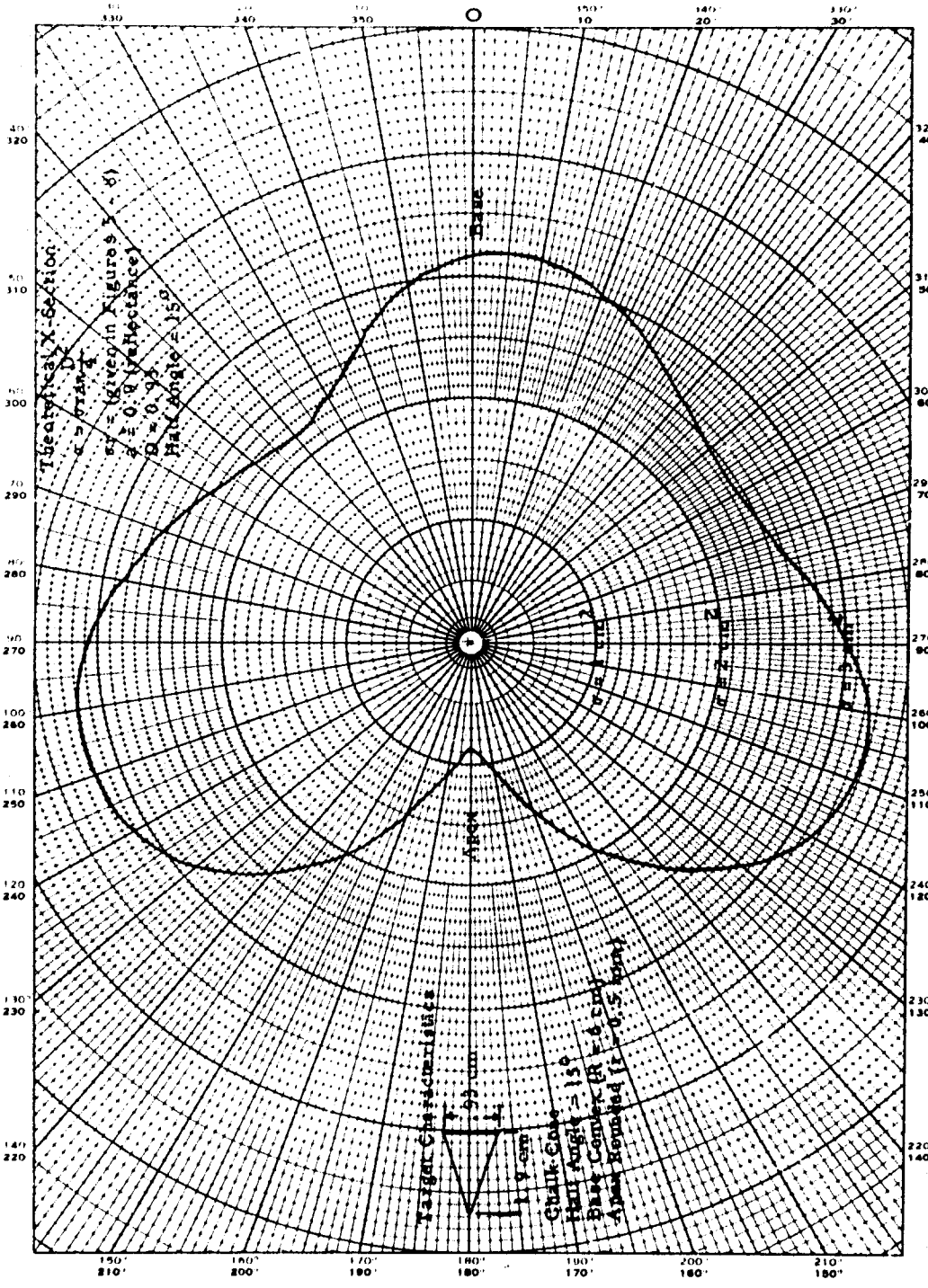

Figure 25. Polar Plot of Experimental Determination for Cross-Section of Chalk Cone.

the traces (particularly the metallic or specular bodies) are quite reproducible and result from slight irregularities in the models. The models are only meant to be illustrative samples and were not machined to any great precision. The data presented is subject to review as no comparison with calculated values have been made for the specular bodies. The expected "σ" for the diffuse sample is noted on Figure 24 by a dashed line. Various mechanical stands and holders in the overall device have recently been modified to permit more degrees of freedom. (See Figure 26.) This will allow a more exact positioning of the sample and photomultipliers.

The light source is being modified to produce a more exact parallel light source and a more uniform distribution of light in the beam cross-section.

5. CHARACTERISTICS OF LASER OUTPUT

5.1 Laser Output

The best possible output (theoretically) from an optical Maser (Laser) should occur when only a single mode of oscillation is present in the Fabry-Perot cavity and all the induced emission is in phase and exactly parallel to the axis of symmetry of the Laser. When these conditions occur, the output from the Laser at large distances should form a Fraunhofer diffraction pattern. For a circular cross-section Laser of radius r the power output at any large range R in vacuo is, according to simple classical theory,

$$p = K \frac{J_1^2 \left(\frac{2\pi r \sin\theta}{\lambda} \right)}{\left(\frac{2\pi r \sin\theta}{\lambda} \right)^2}$$

where

p = power per unit area in direction θ at range R

K = constant of proportionality

r = radius of cylindrical Laser cavity

λ = wavelength of induced emission output

θ = angle off from axis of symmetry of Laser

$J_1(x)$ = the Bessell function of the first kind of order 1.

In order to evaluate the constant K we require conservation of energy which is in equation form (see Figure 27),

$$P_o = \int_o^\infty \int_o^{2\pi} p \rho \, d\rho \, d\phi$$

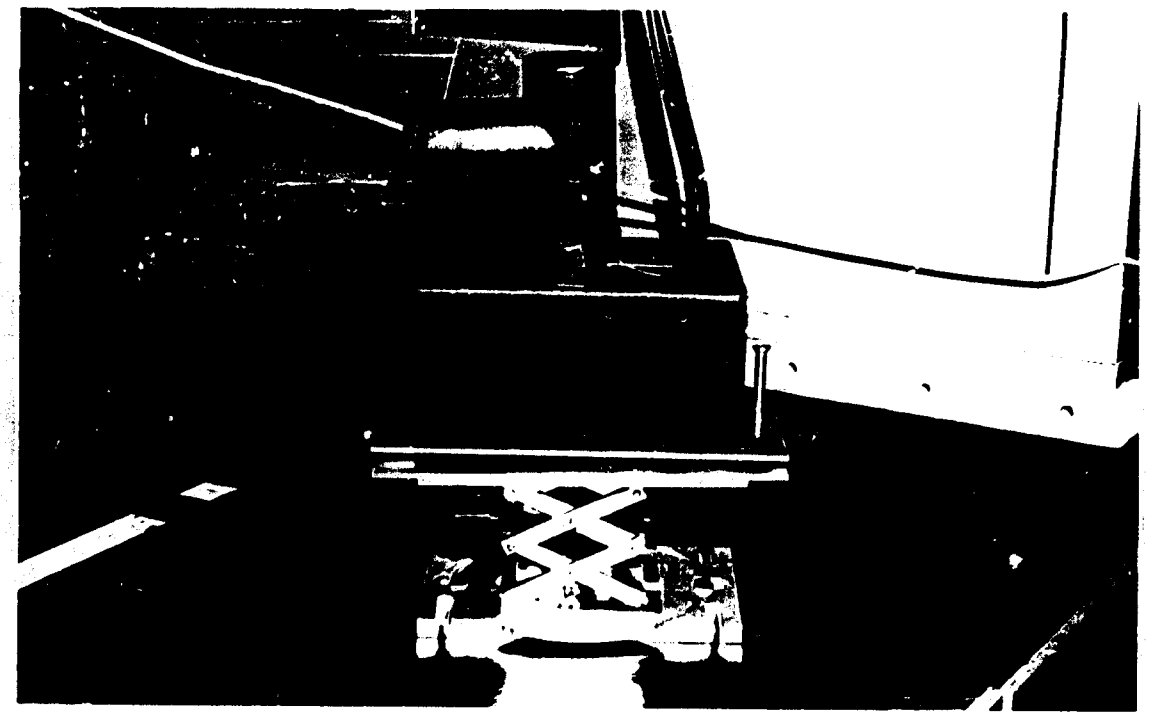

Figure 26. Photograph of Photomultiplier Stand.

where

P_o = the total power output of the Laser

ρ, ϕ = polar coordinates

Assuming 0 is small over the first few fringes, then

$$\sin \theta \approx \tan \theta = \frac{\rho}{R}$$

and

$$P_o = 2\pi \int_o^\infty K \frac{J_1^2 \left(\frac{2\pi r \rho}{R\lambda}\right)}{\left(\frac{2\pi r \rho}{R\lambda}\right)^2} \rho \, d\rho$$

$$= 2\pi \left(\frac{R\lambda}{2\pi r}\right)^2 K \int_o^\infty \frac{J_1^2(x)}{x} \, dx$$

$$= \pi \left(\frac{R\lambda}{2\pi r}\right)^2 K \, .$$

Strictly speaking, this integration should be taken only over the first few fringes where the approximation for sin (θ) is applicable; however, it is known that the maximum value of $\frac{J_1^2(x)}{x}$ (the integrand) goes as x^{-2} for large x. Most of the contribution of the integral comes from the first few fringes. From this we see that

$$K = \frac{P_o}{\pi} \left(\frac{2\pi r}{\lambda R}\right)^2$$

and

$$p = \frac{P_o}{\pi} \left(\frac{2\pi r}{\lambda R}\right)^2 \frac{J_1^2 \left(\frac{2\pi r \sin \theta}{\lambda}\right)}{\left(\frac{2\pi r \sin \theta}{\lambda}\right)^2}$$

Now on axis ($\theta = 0$) and,

$$p_{(o)} = P_o \frac{\pi r^2}{\lambda^2 R^2} \, .$$

If we assume that all of the energy P_o is dumped uniformly into the center fringe, then

$$p_{(o)} = \frac{P_o}{A_1}$$

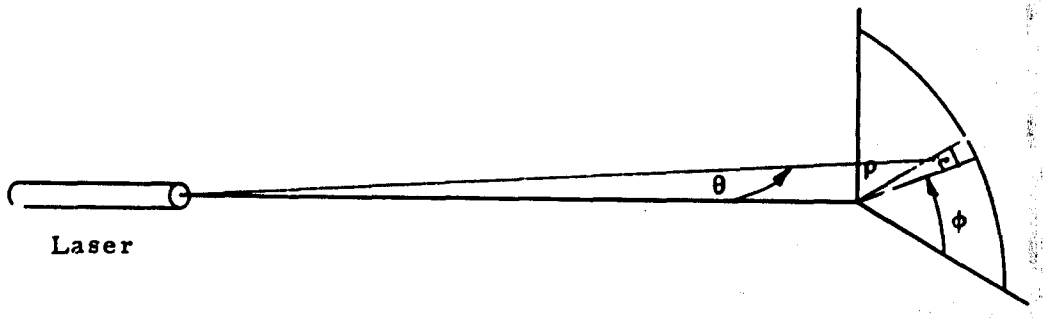

Figure 27. Diagram for Theoretical Determination of Laser Output.

where A_1 is the area of the first fringe.

$$A_1 = \pi(r \tan \theta_1)^2$$

but

$$\frac{2\pi r \sin \theta_1}{\lambda} = 3.83$$

$$\tan \theta_1 \approx \sin \theta_1 = \frac{3.83}{2\pi} \frac{\lambda}{r} = 0.61 \frac{\lambda}{r}$$

and

$$P_{avg.(o)} = \frac{P_o}{\pi R^2} \left(\frac{2\pi r}{3.83\lambda} \right)^2$$

$$= \frac{1}{3.67} \left(P_o \frac{\pi r^2}{\lambda^2 R^2} \right)$$

or only about one quarter as much as at the center of the Fraunhofer diffraction. Better theoretical information about the beam spreading in a large distance can be obtained by vigorous application of coherence theory as developed by Born and Wolff. However, these calculations have not been completed yet since they necessitate a large number of numerical integrations.

It has been reported that the beam widths currently attained are far greater (about an order of magnitude) than the Fraunhofer first dark ring

$$\theta_1 = \frac{0.61\lambda}{r}$$

It appears, therefore, that at present the maximum intensity presently possible with the Laser is about

$$P_{(o)} \approx 10^{-2} P_o \left(\frac{\pi r^2}{\lambda^2 R^2} \right) .$$

A factor of 10^{-2} is used to indicate that there is an increase of 100 in area for an increase of 10 in beam spreading. These findings confirm the anticipation made in Section 2.E.1 of this report. A correlation with the older measurements made on

long distance radar beams and their comparison with diffraction theory should further clarify this problem which is of basic importance to the entire optical radar problem.

5.2 Laser Emission Measurements

A Laser from Power Pac Inc. was received and installed and a number of preliminary shots were made without the crystal to determine proper functioning of the equipment. The crystal was installed and a number of firings were made from which it was determined that the threshold energy level was about 1800 joules.

A phototube system was made for measuring the characteristics of the flash tube and the Laser output. This circuitry consisted of a 925 phototube in series with a 700 volt D.C. power supply and a variable load resistor. The voltage is made high to insure collection of the photoelectrons. The voltage across the load resistor is a measure of the incident flux and is recorded from a high speed 585 Tektronix scope using a Polaroid camera attachment. The load resistor was made variable so that the sensitivity of the instrument and time constant of the circuitry could be varied. At the lowest load resistance the response of the system is in the nanosecond region. Only qualitative output of the flash tube and Laser have been measured at this time. A number of photographs of these oscilloscope traces are shown in Figure 28. To measure quantitatively the total energy output of the Laser, two types of measurements were considered: (1) an integrating type of photocell circuit and (2) a ballistic pendulum for measuring the total radiation pressure impulse which should be proportional to the total energy. Because of the experimental complications and time limitations on the contract, only the integrating phototube circuit was made.

This system consists of a phototube at a high voltage (approximately 700 volts) in series with a capacitor (C). The voltage across the capacitor V(t) is measured with a Tektronix scope with resistance (R). With this arrangement the voltage across the capacitor is:

$$V(t) = \frac{1}{C} e^{\frac{-t}{RC}} \int_0^t i(\tau)\, e^{\frac{\tau}{RC}}\, d\tau$$

where $i(\tau)$ is the time dependent photoelectron current through the tube which, through calibration, should be proportional to the light flux (in ergs/cm^2). Now

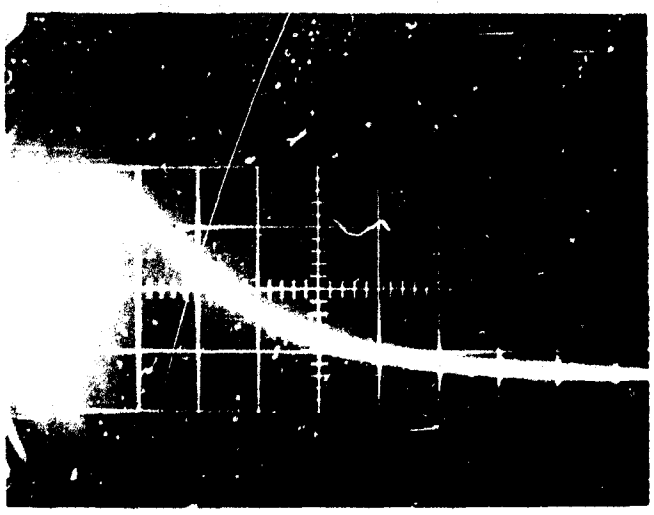

Flash Tube Output 200 μsec/div

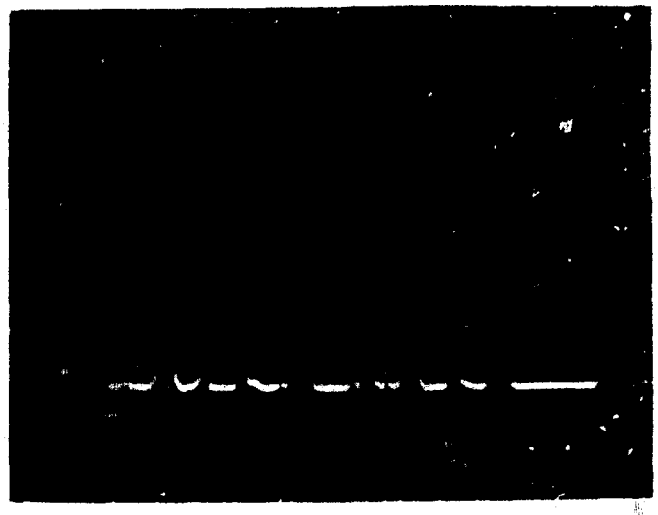

Laser Output, 10 μsec/div

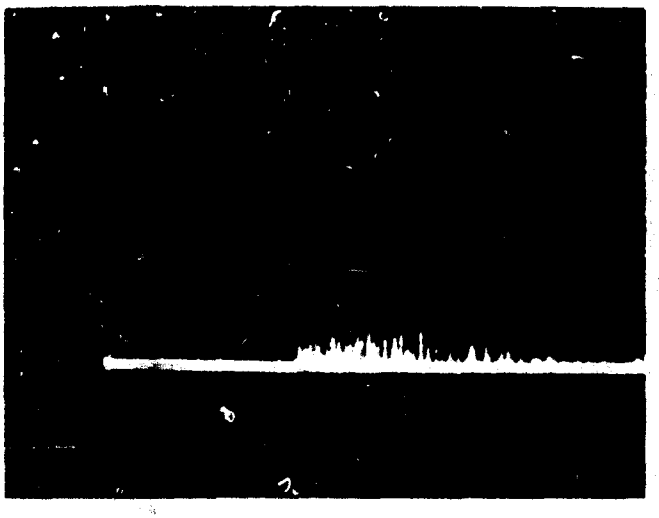

Laser Output 100 μsec/div

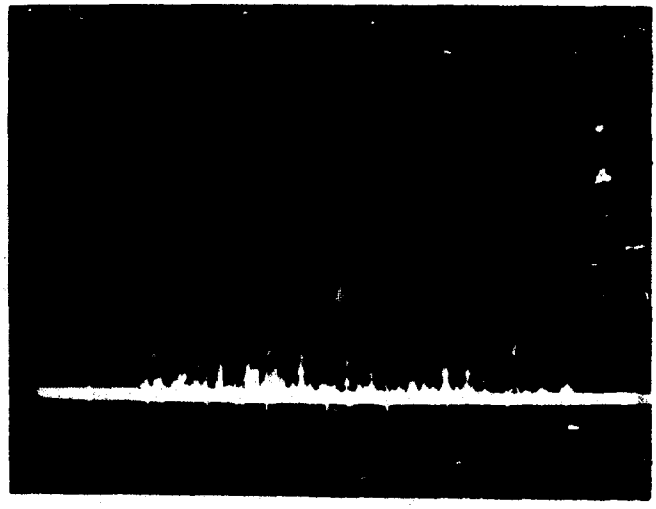

Laser Output 100 μsec/div

Figure 28. Typical Oscilloscope Photographs of Laser and Flash Tube Output

if RC is made large in comparison to $\tau = t_p$, the duration of the pulse, then $\exp(\tau/RC) \approx 1$ for $\tau \leq t_p$, and since $i(\tau) = 0$ for $\tau \geq t_p$, we have

$$V(t) = \frac{1}{C} e^{\frac{-t_p}{RC}} \int_0^{t_p} i(\tau) d\tau = \frac{Q}{C} e^{\frac{-t_p}{RC}}$$

where Q is the total number of photoelectrons collected and measured in coulombs. Since the duration of the Laser flash t_p is about 10^{-3} sec, it will suffice for RC to be about 10^{-1} sec or, since the characteristic impedance of scope R is about 1 megohm, C must be about 0.1 microfarads. The peak voltage of V(t) will then be proportional to the total charge Q.

If we expected a minimum of about 0.001 joule of output energy from the Laser at 6943 Å on the masked off photocathode, this would correspond to about 3.5×10^{15} photons assuming each photon has an energy $\frac{hc}{\lambda}$. Assuming a photoelectronic efficiency of 10^{-2}, there are about 5×10^{-6} coulombs which corresponds to about 50 volts peak across the capacitor. The sensitivity of a 925 phototube at 250 volts is about 1.5×10^{-3} μ amp/μ watt or about 3×10^{-3} electrons per photon at 6943 Å. At 700 volts, the collection efficiency will be much higher, and, for want of a better number, 10^{-2} was used.

Preliminary measurements involving the above were performed, and a series of traces similar to that shown in Figure 29 was obtained. A 925 phototube with power supply of 700 volts and capacitor 0.1 ufd was used. The total input to the Laser was 2250 joules at 3800 volts. A 2.0ND filter was used in front of the phototube for these measurements. The total integrated voltage is seen to be approximately 350 volts considering the attenuator factor of 100. A series of five traces was taken with all controllable parameters remaining constant, and the total integrated voltage was constant within the trace line width representing a maximum deviation of about 10 volts or about 3%. The rate of voltage rise, or the overall trace shape is identical on each to within the trace width. This indicates almost identical energy transfer time relationships between trials.

No quantitative estimates of the total Laser output were made from these preliminary measurements. The output was not confined to the photo surface and the output spatial distribution has not been determined as of this date. It is planned to investigate this procedure further by containing the entire output on the photosurface and by studying the spatial distribution of the output, spectral line widths,

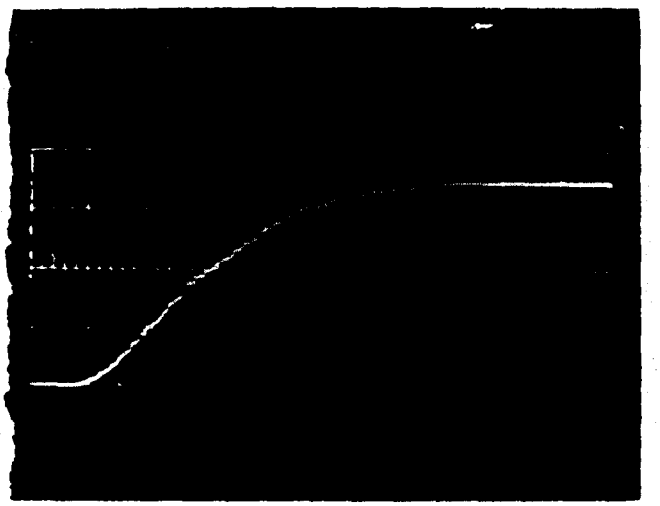

Figure 29. Oscilloscope Photograph of Integrated Laser Output.

effects of optical devices (lens, attenuators, etc.) and phototube collection efficiencies Preliminary phototube calibrations will be made using a calibrated photomultiplier, interference filters, etc. and extrapolating to desired values. Future calibrations should involve the use of higher power light sources, shutters, recording cameras, etc.

5.3 Optical Cross-Sections Using the Laser as a Light Source

Initial determinations of the feasibility of using an experimental arrangement similar to that used in the cross-section measuring photometer have been made. The arrangement is shown in Figure 30 with all shields removed. Each phototube was arranged in a manner similar to the arrangement used for determining the integrated Laser output. No difficulty was experienced in recording the intensity of input light reflected from the glass plate ($\approx 4 \times 10^{-2}$ x input light). The light returned, however, ($\approx 10^{-6}$ x input light) was extremely difficult to record, and only by using flat specular samples could results be obtained. A continuation of this experiment will probably require the use of photomultipliers. The use of integration circuitry will eliminate the need for nanosecond circuitry and amplifiers. Detailed studies of the effects of optical components and a larger range should precede the continuation of this experiment.

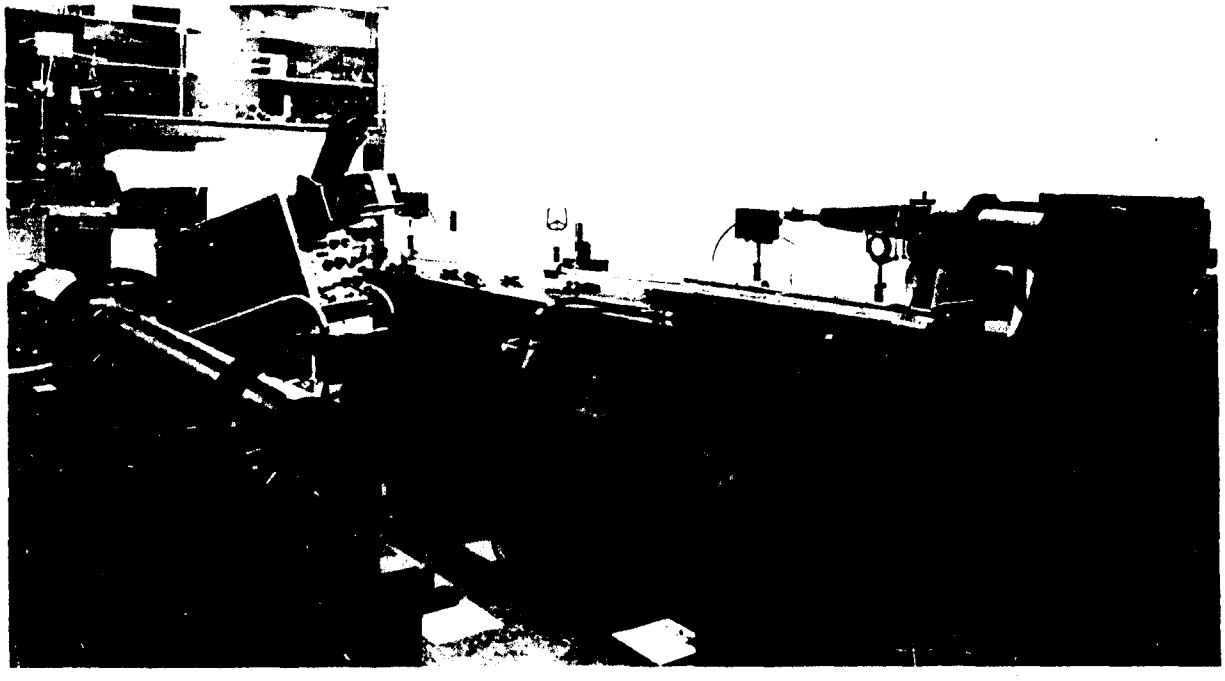

Figure 30. Photograph of Laser Facility and Initial Set-up for Determining Optical Cross-Section.

APPENDIX

LABORATORY FACILITIES

An air conditioned optics laboratory at the University of Dayton was rearranged to facilitate the cross-section photometer; it also contains the Laser light source. Other equipment available for this or related optical experimentation include an Osram 2×10^5 stilb source, a high power carbon arc, a Hilger quartz spectrograph, a Bausch and Lomb 2.5 cm Littrow Spectrograph, a Gaertner precision spectro-goniometer (1 arc sec accuracy), a 9-inch aperture Michelson interferometer, a 5-inch aperture precision polarizer with quarter-wave plates, two 5-inch aperture quartz rotators for plane of polarization measurements, a Soleil compensator (ellipticometer), and a Joyce-Loebl microdensitometer of extreme precision. Electronic equipment suitable for use in optical measurements include a high speed electronic shutter, a nanosecond oscilloscope, an orthicon image tube with associated equipment, and various power supplies suitable for use with photomultipliers, flash tubes, etc. The laboratory also consists of the various optics benches and small optical equipment.

A photographic dark room was established and contains the equipment necessary for film development. This room was used for performing the reflection recording measurements.